CIRCULATION MODELS AND OCEANOGRAPHIC PARAMETERS OF THE NORTHERN GULF OF CALIFORNIA FROM EARTH RESOURCES TECHNOLOGY SATELLITE-1

by

Gustavo Calderon Riveroll

A Thesis Submitted to the Faculty of the

DEPARTMENT OF GEOSCIENCES

In Partial Fulfillment of the Requirements
For the Degree of

MASTER OF SCIENCE

In the Graduate College

THE UNIVERSITY OF ARIZONA

1 9 7 4

STATEMENT BY AUTHOR

This thesis has been submitted in partial fulfillment of requirements for an advanced degree at The University of Arizona and is deposited in the University Library to be made available to borrowers under rules of the Library.

Brief quotations from this thesis are allowable without special permission, provided that accurate acknowledgment of source is made. Requests for permission for extended quotation from or reproduction of this manuscript in whole or in part may be granted by the head of the major department or the Dean of the Graduate College when in his judgment the proposed use of the material is in the interests of scholarship. In all other instances, however, permission must be obtained from the author.

SIGNED: Gustavo Calderón Rivera

APPROVAL BY THESIS DIRECTOR

This thesis has been approved on the date shown below:

L. K. LEPLEY
Assistant Professor of
Arid Land Resources

August 5, 1974
Date

ACKNOWLEDGMENTS

The author wishes to express his appreciation to Dr. Larry K. Lepley, his advisor and thesis director, without whose guidance and assistance this work would not have been possible.

The author also expresses his sincere appreciation to Dr. John R. Hendrickson, Professor of Biology, and to Christine Flanagan, graduate student, for their inestimable help in providing field data, literature, and academic assistance for this project.

This thesis was supported by the Direccion General de Oceanografia y Señalamiento Maritimo (DGOSM) de la Secretaria de Marina and The Consejo Nacional de Ciencia y Tecnologia (CONACYT), Republic of Mexico, and the United States National Aeronautics and Space Administration (NASA) project--A Study of the Marine Environment of the Northern Gulf of California--whose principal investigator was Dr. Hendrickson.

The author also extends his special gratitude to Contralmirante I. E. Gilberto Lopez Lira, Director of DGOSM, to whom he is deeply indebted for his support.

Finally, the author would like to express his gratitude to his wife, Lupita, for her encouragement of the realization of this thesis.

TABLE OF CONTENTS

TABLE OF CONTENTS--Continued

LIST OF ILLUSTRATIONS

LIST OF ILLUSTRATIONS--Continued

LIST OF TABLES

ABSTRACT

Haline and thermodynamic circulation models of the Northern Gulf of California were tested with favorable results against the interpretation of ERTS-1 imagery. The photoanalysis of the data was done in two stages: (a) analysis without surface truth, but assuming the optical properties of the area are known; and (b) analysis using conventional oceanographic and radiometric data collected by the research ship, "Adventyr," during some of the satellite passes. Three enhancement techniques were used in the interpretation of the imagery: (1) color density slicing which improves the differentiation of turbidity levels, (2) color addition which was of limited value for the detection of oceanographic features, and (3) reprocessing of the 70 mm black and white negatives which proved to be necessary to the enhancement of features such as circulation patterns and internal waves. Optical classification of different kinds of sea water was made.

INTRODUCTION

Today studies of the earth have become more sophisticated. Extensive exploration and planned aerial analysis of the earth have been made possible through the modern methods of remote sensing. As it is applied today, remote sensing implies investigation from aircraft, manned and unmanned spacecraft, satellites, and space platforms. This type of investigation consists primarily of measuring characteristics of the surface of the earth through the detection, measuring, and interpretation of electromagnetic radiation of all wavelengths by photographic cameras, multispectral scanners, TV cameras, thermal infra-red sensors, radar systems, radio wave receivers and spectroscopy (Figure 1).

The present phase of remote sensing technology involves the use of artificial satellites equipped with remote sensors.

ERTS-1

On July 23, 1972, the National Aeronautics and Space Administration (NASA) launched a satellite, ERTS-1 (Earth Resources Technology Satellite), into a near-polar orbit. Up to the present, from an orbital altitude of approximately 490 miles, this unmanned satellite continues to obtain detailed imagery coverage of selected test sites around the globe every 18 days provided the sites are not obscured by clouds at the time of its overflight. The Northern Gulf of California, one of these test sites, was chosen for a research project--A Study of the Marine

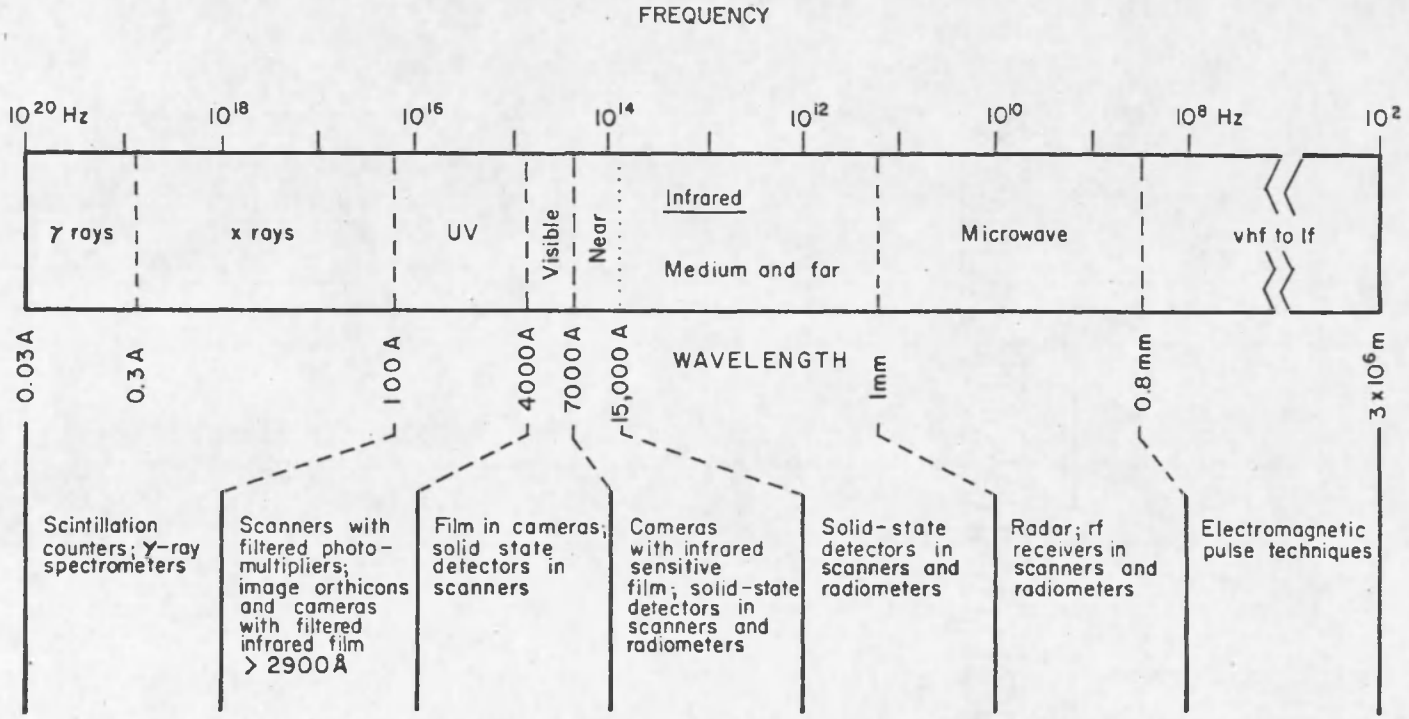

Figure 1. The electromagnetic spectrum and some sensors that use it. -- After Thackrey (1968).

Environment of the Northern Gulf of California. This study was sponsored by NASA and directed by Dr. John R. Hendrickson of the Department of Biological Sciences, The University of Arizona. It had as one of its purposes, the testing of the feasibility of ERTS-1 monitoring of oceanographic parameters as well as its seasonal variations (Hendrickson 1973). This thesis was developed for the above purpose and has as its primary objective the photoanalysis of one year's data of ERTS-1 imagery of the Northern Gulf of California (August 1972 to July 1973) from a physical oceanographic point of view. Therefore some parts of this study have been published in previous reports (Lepley, Hendrickson and Calderon 1973).

Importance of the Study

In recent years the Northern Gulf of California has been the subject of a series of investigations involving several disciplines. The reasons for this are:

1. The flow of the Colorado River, as recorded at Yuma, Arizona, has been reduced from an average annual flow of 15,094,000 acre feet (1902-1934) to 4,380,059 acre feet (1935-1963; see Schreiber 1969a). The effects of this flow reduction on the Northern Gulf of California still need to be documented.
2. The most important industry in the Northern Gulf of California area is fishing. In the past ten years, this industry has suffered major changes that are still largely unexplained. Therefore, all information on the oceanography of the area is of great interest to those seeking answers to this important problem.

3. Because of the clear, cloud-free atmosphere which generally prevails over the Northern Gulf of California, it is considered to be an ideal test site to demonstrate the feasibility of ERTS-1 monitoring of the environment.
4. The Northern Gulf of California and the San Andreas fault are considered to be the boundary between the Pacific and North America tectonic plates, even though some aspects of this theory still need to be confirmed.

DESCRIPTION OF THE AREA OF STUDY

The area of investigation is defined in Figure 2. It lies between 31°10' and 32°00' North latitude and longitudinally between the east and west shorelines of the Gulf of California.

Schreiber (1969b, pp. 3-5) gives a good description of the area:

> This somewhat triangular area is formed by the Gulf ports of San Felipe, Puerto Penasco, and the Colorado River delta. The west side is in the state of Baja California and is flanked by the Sierra San Pedro Martir and lesser ranges. These ranges consist chiefly of pre-Cretaceous and Cretaceous igneous and metamorphic rocks (Beal 1948). The low-lying coastal plain area between San Felipe and the mouth of the Colorado River consists of barren mud and salt flats whose sediment was derived from the Colorado River. The sediments are silt and clay and evaporites of recent age, but sediments of Pleistocene age have also been recognized in the area (Thompson 1965).
>
> The northeast side is in the Sonoran Desert which grades northward into the Colorado Desert. The Sonoran Desert along this side of the Gulf has also been designated the Gran Desierto and the Desierto del Altar. Near the coast, the desert consists of an alluvial plain of bedded sand and gravel which is covered in places by sand dunes. The geologic map of Mexico (Comite de la Carta Geologica de Mexico 1960) shows this desert area to consist chiefly of Pleistocene and Recent sediments, late Cenozoic clastic sediments and volcanics, and granites of Mesozoic and Precambrian age. Pelican Point, a few miles west of Puerto Penasco, consists of a light-colored granite of Mesozoic age laced with pegmatite and aplite dikes. Punta Penasco, the dark hill at Puerto Penasco, and Black Mountain, located west of Pelican Point, are basalt. The Pinacate region, a basaltic volcanic field, occupies about 600 square miles of the desert country 55 km north of Puerto Penasco and 65 km west of Lukeville, Arizona.

Figure 3 shows the area of study and its surroundings. The delta area has been described by Thompson (1965, pp. 6-7):

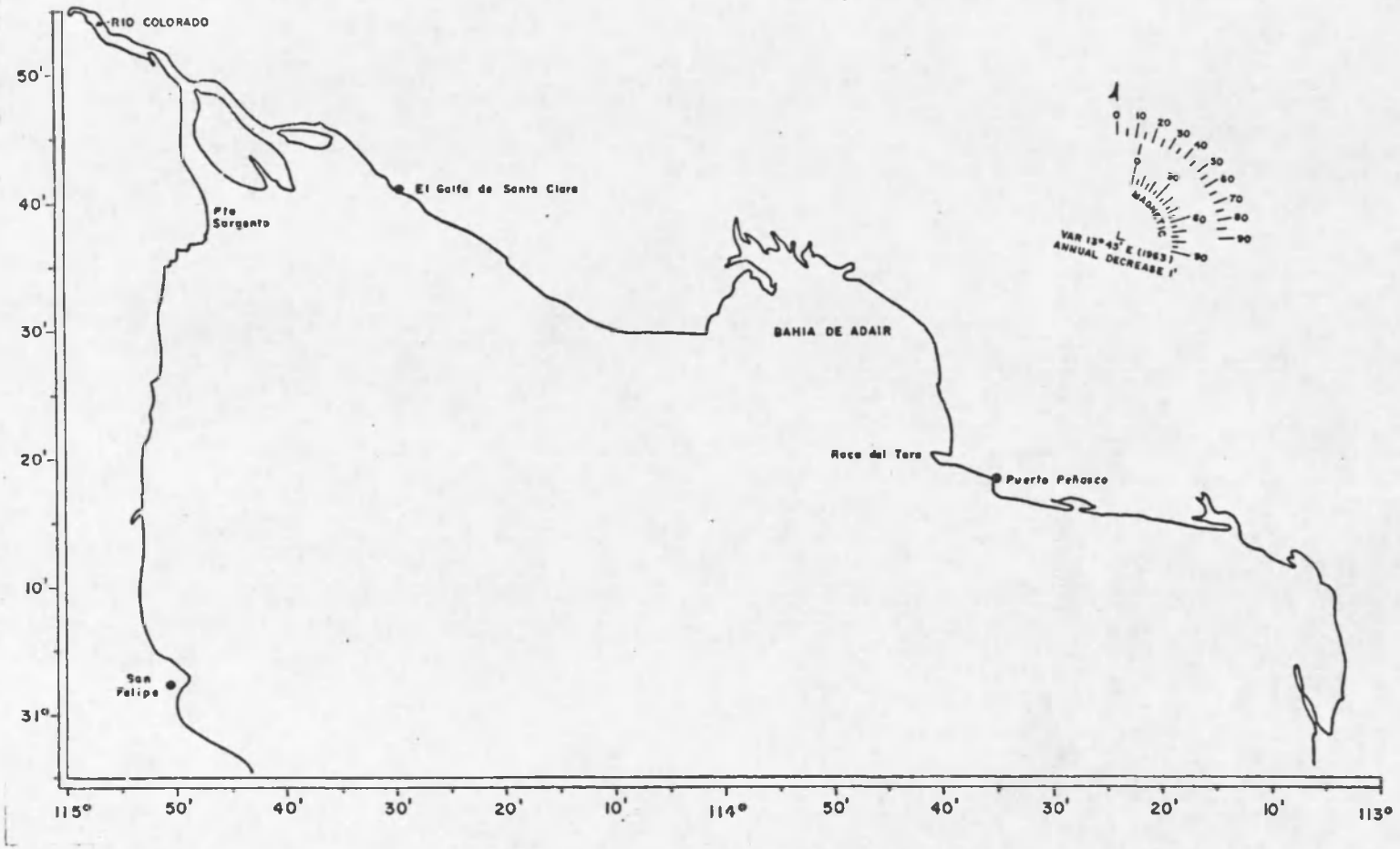

Figure 2. Area of investigation.

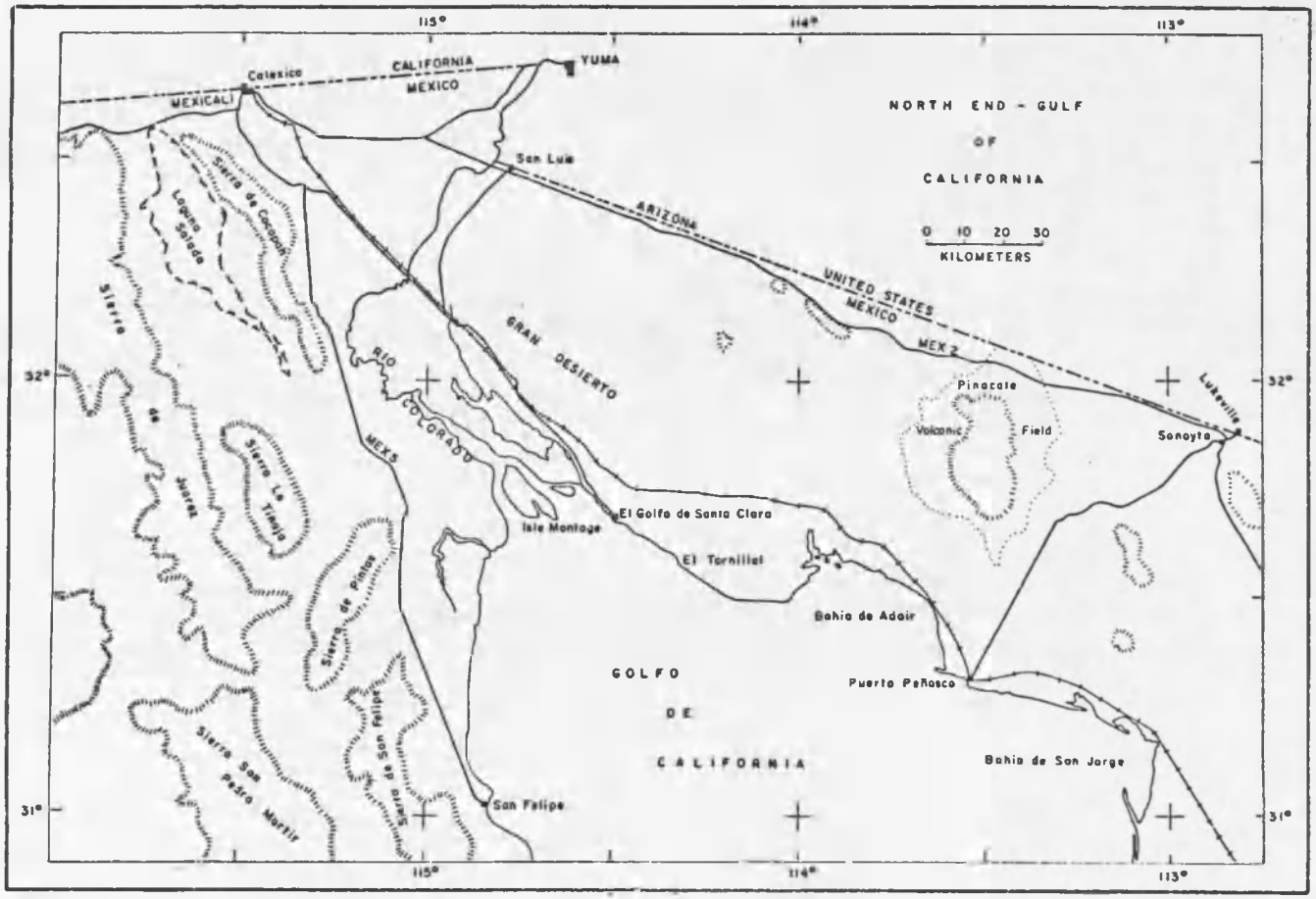

Figure 3. Area of study and its surroundings. -- After Schreiber (1969b).

The crest of the present deltaic cone trends southwestward from an elevation of 43 m near Yuma, Arizona, to a minimum elevation of about 11 m near Cerro Prieto, 25 km south of Mexicali, Baja California. To the north, the delta surface slopes into the Salton Basin at a gradient of approximately 0.8 m/km. On the Gulf side, the deltaic cone dips southwestward at a gradient of 0.35 m/km to the 5 m contour at a latitude 32° North. Former meander belts, levees, and extensive secondary deltaic cones bear witness to the dominant influence of fluvial processes in this sector. Surface deposits are generally sandy, and under natural conditions were covered by dense vegetation (Sykes 1937).

Southeast of the 5 m contour, the influence of the high Gulf tides is apparent. The delta surface maintains a very low gradient of about 0.016 m/km to the higher high tide line near the river mouth. This section is characterized by barren mud and salt flats, which are transected only by the relatively straight estuary of the river.

Bathymetry and Bottom Topography

In the southern part of the area, depths as great as 200 meters are found (Wagner Basin), while in the northern part, above Consaga Rock, sediments from the Colorado River have reduced the depth to less than 20 meters. Figure 4 shows a bathymetric map of the Northwestern Gulf of California compiled by Thompson (1965).

The western part of the area is characterized by a smooth and plain bottom topography with an average gradient of 0.05° from mean sea level to depths of about 15 m (Thompson 1969b). This kind of topography represents the subtidal continuation of the intertidal mud flats that have accumulated along the western coast from the Colorado River Estuary to near San Felipe.

The bottom topography of the eastern part of the area is characterized by low ridges and intervening flat-bottomed troughs. These ridges and troughs are best developed near the mouth of the Colorado

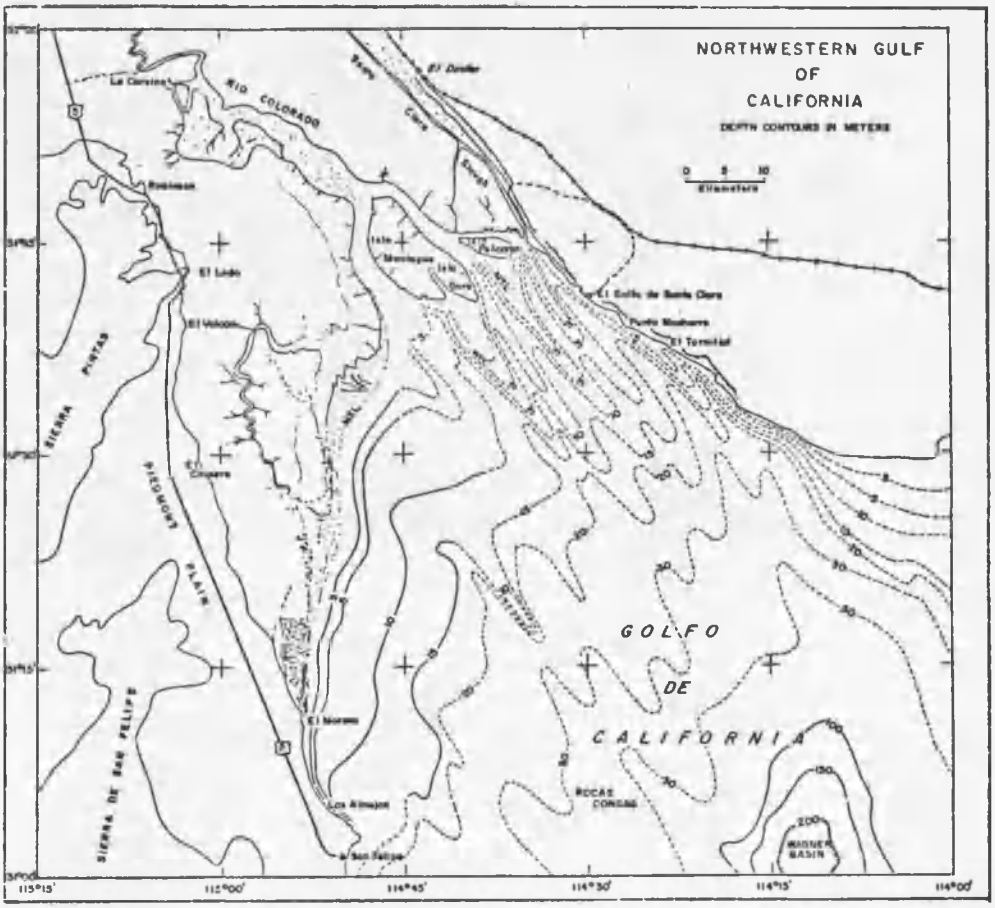

Figure 4. Bathymetry of the Northwestern Gulf of California. -- After Thompson (1965).

River and are thought to represent tidal current ridges formed by the strong tidal currents observed in the area (Thompson 1969b).

A singular topographic feature is well delineated in the eastern part of the Northern Gulf. This feature consists of a prominent submarine channel that runs from the eastern tip of Isla Pelicano to the north end of the Wagner Basin. This channel is thought to represent a former entrenched course of the Colorado River (Thompson 1969b).

Along the Sonoran coast, the bottom topography is represented by irregular troughs separated by shoal ridges. Water depths of 25 to 30 meters are encountered very close to the shore line, in contrast with the plain bottom topography of the western gulf. The irregular topography close to the Sonoran coast is said to be the result of the combined effects of former river cutting and recent crustal disturbances along the San Jacinto fault which extends into this area from the northwest.

Surface Sediments

The distribution of surface sediments in the Northern Gulf of California has been described by Thompson (Thompson 1969a, pp. 74-76):

> Surface sediments in the northwestern Gulf of California fall principally into the textural categories of silty clay, sand-silt-clay, and sand, with relatively minor occurrences of muddy sand and clayey silt (Figure 5). Silty clay predominates over most of the intertidal mud flats north of San Felipe and covers the smooth subtidal plain in the Western Gulf, to depths of 10-12 m. Petrography of these sediments has been studied in detail by Thompson (1965). The Wagner Basin and deeper area immediately west thereof are also characterized by silty clay. These clays are brownish gray in color, homogeneous in appearance, and average about 5 percent sand, 40 percent silt, and 55 percent clay.

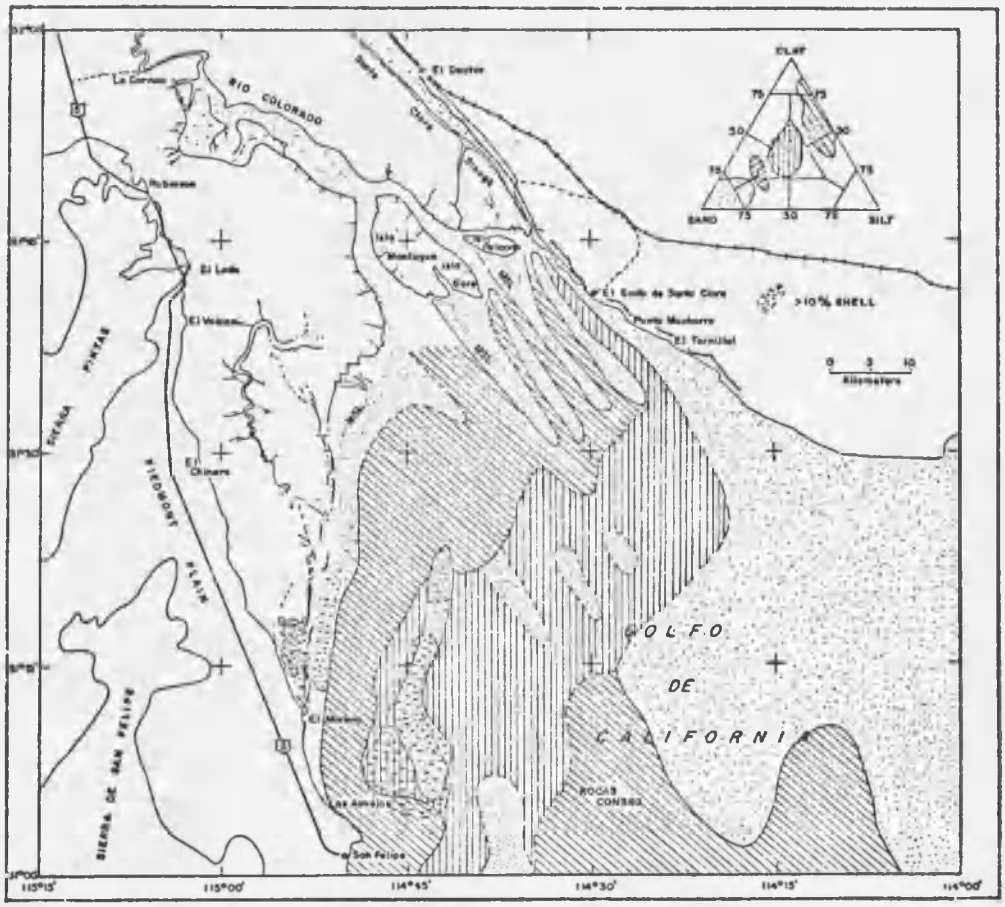

Figure 5. Surface sediments of the Northwestern Gulf of California. -- After Thompson (1969b).

> Fine to medium sand occurs in a continuous belt along the Sonoran coast extending throughout the intertidal and shallow subtidal zone. This belt widens southward and merges with an extensive area of sand covering the shelf north and east of the Wagner Basin. Much of this sand is believed to be relict, left uncovered since the last Wisconsin rise of sea level.
>
> In the remainder of the northwestern Gulf, the textural distribution is complicated, and appears to be controlled by the irregular morphology. Near the mouth of the Colorado River clean, fine sand prevails on the crests of the tidal current ridges and silty clay is found in the intervening troughs. Further south, slightly muddy sand occurs only on the higher ridges, while sand-silt, clay covers the lower ridges and troughs. The overall textural pattern in the northwestern Gulf is that of predominantly sand on the east, predominantly silty clay on the west, and a zone of mixed sediments in between.

The source of these sediments is the Colorado River, according to a study made by Thompson in 1965. However, it is necessary to mention that in the last 60 years due to man's activity, the Colorado River has supplied a very small amount of sediment to the Gulf.

Tides

The size and shape of the Gulf of California provides a resonant system to the semi-diurnal tidal cycle, with the result that a 9-10 meter tidal range is found in the northern reaches of the Gulf (Matthews 1969, Filloux 1972).

MULTISPECTRAL IMAGERY APPLIED IN OCEANOGRAPHY

In 1968, Dr. Larry K. Lepley compiled and extrapolated Naval Oceanographic Office Secchi disk transparency data to show the global distribution of coastal water clarity. He found that 50 percent of the world's coastlines have 70 to 90 percent transmission per meter (depths of 5 to 20 m). Coastal waters with more than 92 percent transmission (over 20 m depth) comprise 35 percent; and 10 percent of the total has a transmission better than 30 meters. The spectral range considered varies from about 450 mμ to 580 mμ. These findings together with the analysis of several of the 70 mm color and multiband photographs taken by the astronauts during the Gemini and Apollo flights have shown that space imagery can be used for studying sea water types (Mairs 1970).

Among remote image-forming sensors which are used in the remote-sensing programs for oceanography, good spatial resolution is provided by the multiband camera and the multispectral scanner. Even more important, they are the only sensors which directly record information below the surface of the ocean with this order of resolution.

Multispectral imagery is of great importance in the different aspects of oceanography. The hydrographer is concerned with keeping his charts up to date to meet the rapidly increasing demands of ocean commerce and resources development (Badgley, Miloy and Childs 1968). The biologist is concerned with the correlation that exists between

oceanic chlorophyll concentration and the ocean's color spectrum, as an indication of the water's productivity (Duntley 1972). The marine ecologist is interested in detecting pollution in the oceans by correlating the variation of skylight reflectance with oil and other pollutants in the seawater (Badgley et al. 1968). The physical oceanographer is interested in detecting circulation, currents, tidal and internal wave patterns, color boundaries as indicative of different water masses, and turbidity levels (Merrit and Stancioff 1971). At present, multispectral imagery has become the main optical tool for gathering information in the visible and near infrared region for its use in the above-mentioned branches of oceanography. Table 1 presents a summary of the optical multispectral sensors that may be used from spacecraft to study different kinds of marine features.

Characteristics of Oceanographic Subjects

Except for shorelines and similar features which vary sharply in color or form from the surrounding terrain, the oceanographer is concerned primarily with recognizing and interpreting the meaning of very slight changes in color hue and color saturation evident in the color photograph or the multispectral record.

In oceanography, information of vital scientific and economic importance is in the .460-.510 and .510-.560 micron bands (Ross 1969); information on water clarity, color, biological activity, depth, bottom composition and topography, currents, sediment transport and many other features are found in the blue-green region. In coastal water the peak of upwelling light in the water may shift toward yellow, but the

Table 1. Application of multispectral imagery to oceanography.

Features to be Measured	Instrument	Wavelength
Sea surface thermal mapping	Optical Mechanical Scanner	3-5.5 μm and 8-13 μm
Ice surveillance	Multiband camera, Optical Mechanical Scanner	.4-.7 μm 8-13 μm
Interface land/water	Optical Mechanical Scanner	.7-1.1 μm
Fresh/salt water	Multiband camera, Optical Mechanical Scanner	.4-1.1 μm
Water pollution	Multiband camera, Optical Mechanical Scanner	.4-1.1 μm
Suspended sediments	Multiband camera, Optical Mechanical Scanner	.4-1.1 μm
Shoals and coastal mapping	Multiband camera, Photography, and Optical Mechanical Scanner	.4-1.1 μm
Currents	Multiband camera, Photography, and Optical Mechanical Scanner	.4-13 μm
Coastal marine processes: shore and water lines at various tidal stages	Multiband camera, Photography, and Optical Mechanical Scanner	.4-1.1 μm
Ocean waves	Photography	.4-.7 μm
Biological: Bioluminescence Red tides Plankton Chlorophyll Schools of fish	Photography, Multiband camera, and Optical Mechanical Scanner	.4-.7 μm

interpretation problem is that of detecting slight changes within a relatively narrow spectral band.

The energy for image-formation is supplied by sunlight. Figure 6 is a schematic diagram outlining the major factors which influence the scattering and absorption of sunlight in the atmosphere and in the ocean, and which serve to spectrally modify and attenuate the contrast of image flux reaching the sensor.

Ocean Spectral Data

One of the most difficult problems associated with the interpretation of remote spectral measurements of the ocean is the separation of atmospheric effects from the signal which originates in the water. The total signal received by a high altitude aircraft or spacecraft contains information originating in both the water and in the atmosphere, with the latter predominating (White 1972). Thus the signal received by the sensor is:

$$S_T = S_A + S_W$$

where S_T, S_A and S_W are the signals received at the sensor, the individual components from the atmosphere, and the water, respectively. S_A is larger compared to S_W and is typically larger by a factor of 10 in the case of a spacecraft measurement. Thus, an uncertainty of one percent in S_T can result in an uncertainty of 10 percent in deriving S_W.

This imposes severe accuracy and sensitivity requirements on the measurement of S_T and on the calibration of the instruments which make these measurements.

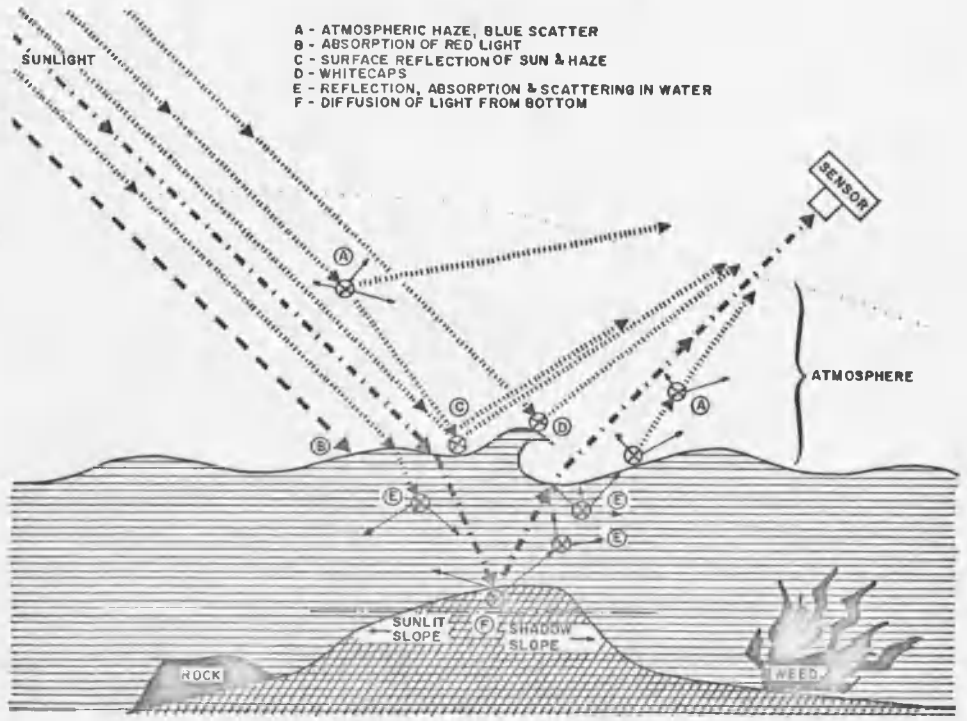

Figure 6. Scattering, absorption, and contrast attenuation image flux by atmosphere and water. -- After Badgley et al. (1968).

Necessity of Surface Truth

Multispectral imagers sense directly only the apparent spectral radiance of oceanographic features. This apparent number can lead to some qualitative determinations, but, because it is not an inherent feature property, it is usually difficult to interpret any significant information from this quantity. As a result, it is necessary to acquire information in some other way in order to be able to interpret what this remotely measured spectral radiance means. This is the purpose of ground truth.

The remotely sensed apparent spectral radiance is determined directly by four things:

1. Reflectivity or emissivity.
2. Illumination.
3. Temperature.
4. Atmospheric path effects.

The first three items determine the actual spectral radiance of the feature. The last item determines how the atmospheric path between the ocean surface and sensor alters the actual radiance to produce an apparent radiance. Of these four parameters influencing the apparent radiance sensed, items 1 and 3 are the ones which the scientist would most like to know since these parameters are properties of the target and thus contain the ultimate information sought.

All of these quantities vary according to target type, target condition, and the environment as shown in Table 2. In the case of the

Table 2. Factors determining the remotely sensed apparent spectral radiance of water features.

Remotely Observed Quantity	Determined Directly By	Which is Influence By
Apparent Spectral Radiance	Reclectivity/Emissivity	Water type Water condition
	Illumination	Environment
	Temperature	Water type Water condition Environment
	Atmospheric Effects	Environment

ocean, these parameters are described by observing or measuring the following quantities.

Environment

a. Solar radiance intensity.

b. Atmospheric thermal radiation intensity.

c. Cloud cover.

d. Air temperature.

e. Wind speed and direction.

f. Water vapor content or air.

g. Atmospheric contaminants (dust, haze).

Water type and condition

a. Transparency.

b. Suspended matter.

c. Turbidity.

d. Illumination.

e. Surface temperature.

f. Reflectivity, emissivity.

ERTS-1 SENSORS

The ERTS-1 spacecraft (Figure 7) carries two types of imaging sensors: the Return Beam Vidicon (RBV) cameras and the Multispectral Scanner (MSS). The Return Beam Vidicon cameras are television cameras mounted side by side in the spacecraft and bore-sighted to simultaneously photograph the earth beneath the spacecraft in each of three spectral regions (Table 3). The individual frames of RBV images cover approximately 100 x 100 nautical miles and overlap by 10 percent along the spacecraft track.

The multispectral scanner (MSS) is a line scanning device--a radiometer which measures the spatial distribution of radiation from a source by moving the field of view of the optical system before the radiation is dispersed and focused into four solid state detectors--which uses an oscillating mirror (Figure 8) to simultaneously scan the terrain passing beneath the spacecraft in four spectral bands (Table 3). As in the case of the RBV's the electronic signals are converted to 70 mm system corrected images.[1] The image scale is approximately 1:3,369,000 and the swath width is approximately 100 nautical miles wide. Although the scanner data are acquired in a continuous swath, in the process of electronic signals to image conversion the images are

---

1. Imagery that contains the radiometric and initial spatial corrections introduced during the process of video tape to film conversion.

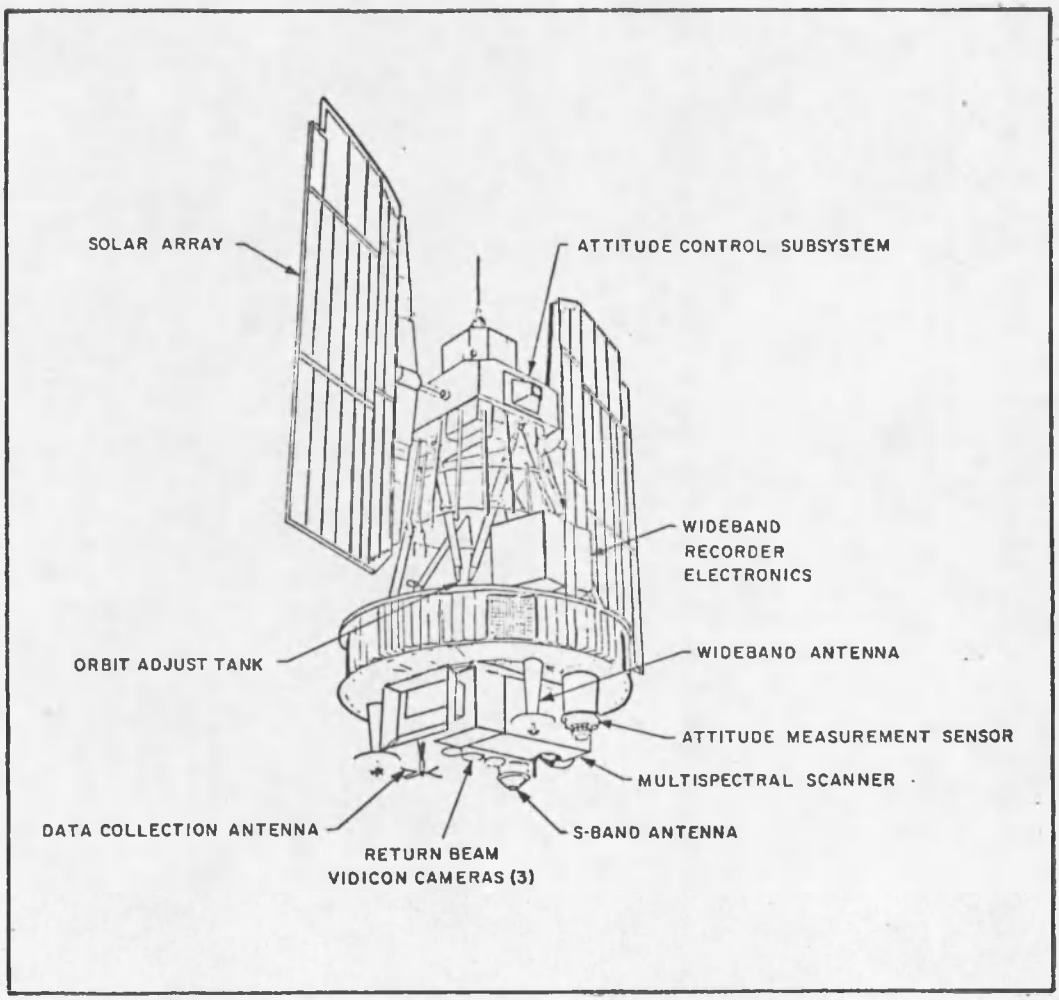

Figure 7. ERTS-1 spacecraft. -- After NASA (1972).

Table 3. ERTS-1 sensors spectral bands.

Sensor	Wavelengths (Micrometers)	EM Spectrum Position	Band Code
RBV	.475-.575	Visible (green)	1
	.580-.680	Visible (red)	2
	.690-.830	IR*	3
MSS	.500-.600	Visible (green)	4
	.600-.700	Visible (red)	5
	.700-.800	IR*	6
	.800-1.1	IR*	7

* NOTE: The IR bands of these sensors are known as solar IR bands. Therefore, they have nothing to do with the scene thermal properties.

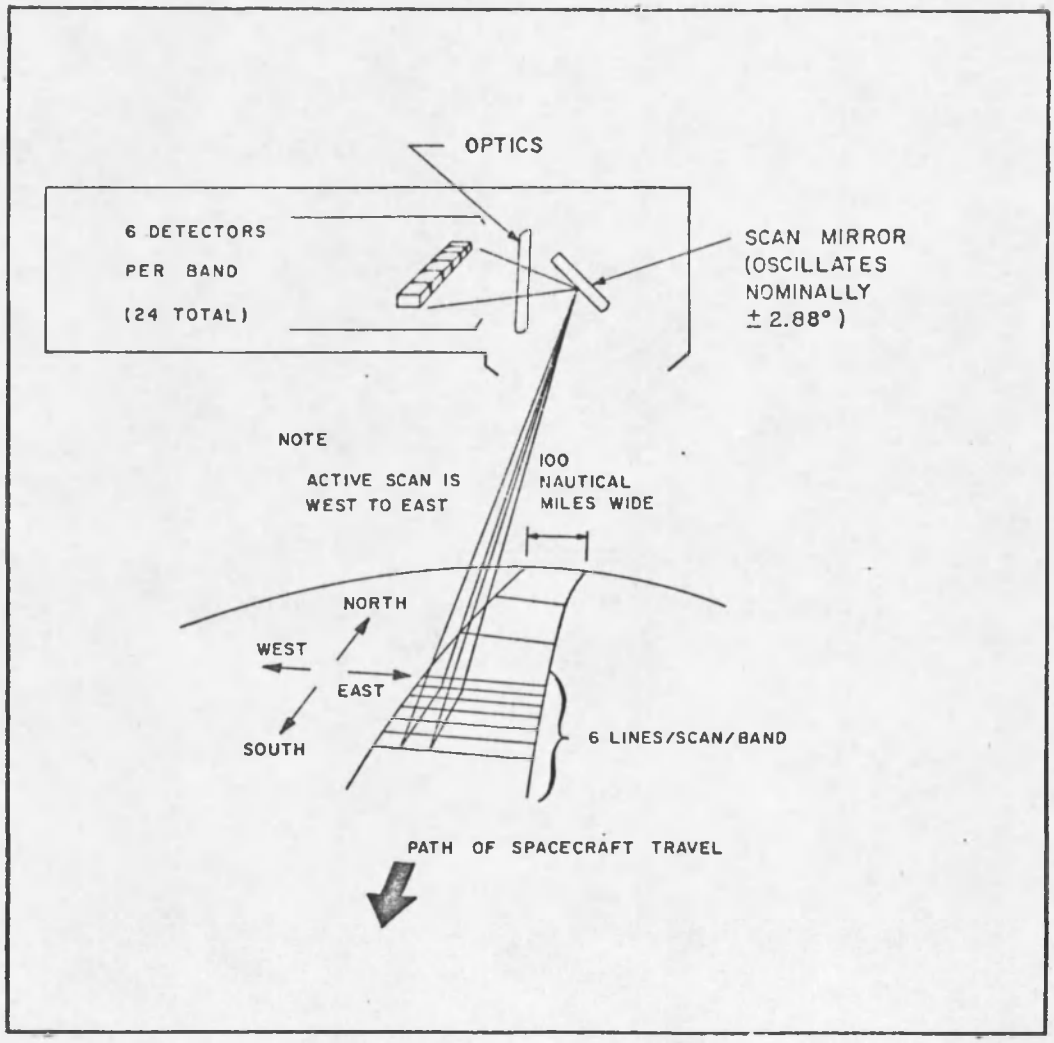

Figure 8. ERTS-1 Multispectral scanner operation. -- After NASA (1972).

divided into frames to correspond with the frame coverage of the RBV camera. A detailed description of the operation and the photographic products of the ERTS-1 satellite can be found in the ERTS-1 user's manual (NASA 1972).

Of the two sensors carried aboard the satellite (RBV and MSS), only the MSS is now being used. An electronic failure in the RBV power supply circuitry in August, 1972, made it difficult to switch between the two imaging systems, and the RBV was shut down.

Comparison of the MSS with Photographic Cameras

Multispectral images in the visible region and in the infrared can be obtained both by cameras and by scanners. Aerial photographic systems are quite fine for establishing the positions of sources so that accurate maps can be made. Reconnaissance cameras can provide detailed recordings of the distribution in black and white as well as color and false color forms. Satellite based cameras can provide important geological information with relatively inexpensive photographic equipment. With such demonstrated capacity to record positional distribution of radiation what is the need to utilize a multispectral scanning apparatus in ERTS-1?

The principle reason is that both spectral and spatial radiometric measurements with a high degree of accuracy can be obtained in a form suitable for analysis by high speed computation methods when optical mechanical scanners are used. The photographic process is seriously limited in: (1) precision--the multiple steps to produce the image and

the tendency of the process to become nonlinear in almost every property makes reproducible quantitative results very difficult to achieve. (2) Spectral range--the photographic process is limited to wavelengths shorter than one micron by self-exposures due to its own internal radiation. (3) Computational form--the spectral-spatial information is in the form of silver on dye deposits while the high speed computation equipment requires electrical signals with spectral data accurately correlated with position in the scene. The multispectral scanner overcomes these limitations, but loses some of the positional accuracy needed for standard mapping purposes.

DATA ANALYSIS

The interpretation of the ERTS-1 imagery supplied for the study was done in two stages:

1. Imagery evaluation without ground truth, but using some background knowledge about the area.
2. Imagery evaluation using ground truth data gathered by the research ship, "Adventyr."

Imagery Selection

The imagery used for the photoanalysis (Table 4) was selected according to the following criteria:

1. Availability of the imagery.
2. Good quality.
3. Cloud coverage of less than 30 percent.

ERTS-1 Imagery Products Used for the Analysis

As shown in Table 4, the ERTS-1 imagery products used in the photoanalysis were:

1. 70 mm negatives.
2. 70 mm positives.
3. 9.5 inch positive.
4. 9.5 inch dodged prints.

Table 4. ERTS-1 imagery analyzed.

Date	Frame ID Orbit No.	Time (GMT)	Bands	70 mm. pos.	70 mm. neg.	9.5" pos.
8/ 7/72	1015	17442	4,5,6,7	x	x	x
8/24/72	1032	17391	4,5,6,7	x	x	x
8/25/72	1033	17444	4,5,6,7	x	x	x
9/11/72	1050	17385	4,5,6,7	x	x	x
9/11/72	1050	17392	4,5,6,7	x	x	x
9/12/72	1051	17443	4,5,6,7	x	x	x
9/12/72	1051	17450	4,5,6,7	x	x	x
9/29/72	1068	17385	4,5,6,7	x	x	x
9/29/72	1068	17391	4,5,6,7	x	x	x
9/30/72	1069	17443	4,5,6,7	x	x	x
9/30/72	1069	17450	4,5,6,7	x	x	x
11/ 4/72	1104	17393	4,5,6,7	x	x	x
11/ 5/72	1105	17452	4,5,6,7	x	x	x
12/29/72	1159	17451	4,5,6,7	x	x	x
12/29/72	1159	17454	4,5,6,7	x	x	x
2/ 2/73	1194	17400	4,5,6,7	x	x	x
2/ 3/73	1195	17452	4,5,6,7	x	x	x
2/ 3/73	1195	17455	4,5,6,7	x	x	x
3/10/73	1230	17400	4,5,6,7	x	x	x
3/10/73	1230	17402	4,5,6,7	x	x	x
3/11/73	1231	17454	4,5,6,7	x	x	x
3/28/73	1248	17400	4,5,6,7	x	x	x
3/28/73	1248	17408	4,5,6,7	x	x	x
3/29/73	1249	17455	4,5,6,7	x	x	x
3/29/73	1249	17461	4,5,6,7	x	x	x
4/15/73	1266	17400	4,5,6,7	x	x	x
4/15/73	1266	17402	4,5,6,7	x	x	x
4/16/73	1267	17454	4,5,6,7	x	x	x
4/16/73	1267	17461	4,5,6,7	x	x	x
5/ 3/73	1284	17395	4,5,6,7	x	x	x
5/ 3/73	1284	17402	4,5,6,7	x	x	x
5/ 4/73	1285	17454	4,5,6,7	x	x	x
5/ 4/73	1285	17460	4,5,6,7	x	x	x
5/21/73	1302	17394	4,5,6,7	x	x	x
5/21/73	1302	17401	4,5,6,7	x	x	x
5/22/73	1303	17453	4,5,6,7	x	x	x
5/22/73	1303	17455	4,5,6,7	x	x	x
6/ 8/73	1320	17393	4,5,6,7	x	x	x
6/ 8/73	1320	17395	4,5,6,7	x	x	x
6/ 9/73	1321	17451	4,5,6,7	x	x	x
6/ 9/73	1321	17454	4,5,6,7	x	x	x
6/26/73	1338	17392	4,5,6,7	x	x	x
6/26/73	1338	17394	4,5,6,7	x	x	x
6/27/73	1339	17450	4,5,6,7	x	x	x
6/27/73	1339	17453	4,5,6,7	x	x	x
7/14/73	1356	17390	4,5,6,7	x	x	x
7/14/73	1356	17393	4,5,6,7	x	x	x
7/15/73	1357	17445	4,5,6,7	x	x	x
7/15/73	1357	17451	4,5,6,7	x	x	x

Figure 9 shows an example of the kind of data supplied by the MSS. This print cluster of the four MSS bands was obtained from the 70 mm negatives of the data corresponding to the December 29, 1972, satellite overpass. This cluster is a good example of the contrast that may be expected among the four frames due to the different spectral bands they represent (Table 3). Band number 4 (.500 to .600 micron) shows low tonal contrast between the submerged and exposed land, but gives good information about clear waters (darker areas in the photo). This band also shows the greatest atmospheric and water haze effect. Band number 5 (.600 to .700 micron) shows the best tonal contrast in the water itself permitting the identification of several water features. Finally, bands 6 and 7 (.700 to .800 and .800 to 1.1 micron) give the best information about the interface sea-land, deltaic areas and delineate quite well the bodies of water existent in the surrounding area.

Imagery Evaluation without Ground Truth

Background

Before the photoanalysis started, some facts about the area were assumed:

1. The tidal excursions in the Gulf are very intense, ranging up to 10 meters between low and high tides (Filloux 1972, Matthews 1969, Thomson 1972).
2. The tidal currents are extremely rapid (Matthews 1969).
3. The lack of outflow of the Colorado River (Schreiber 1969a).

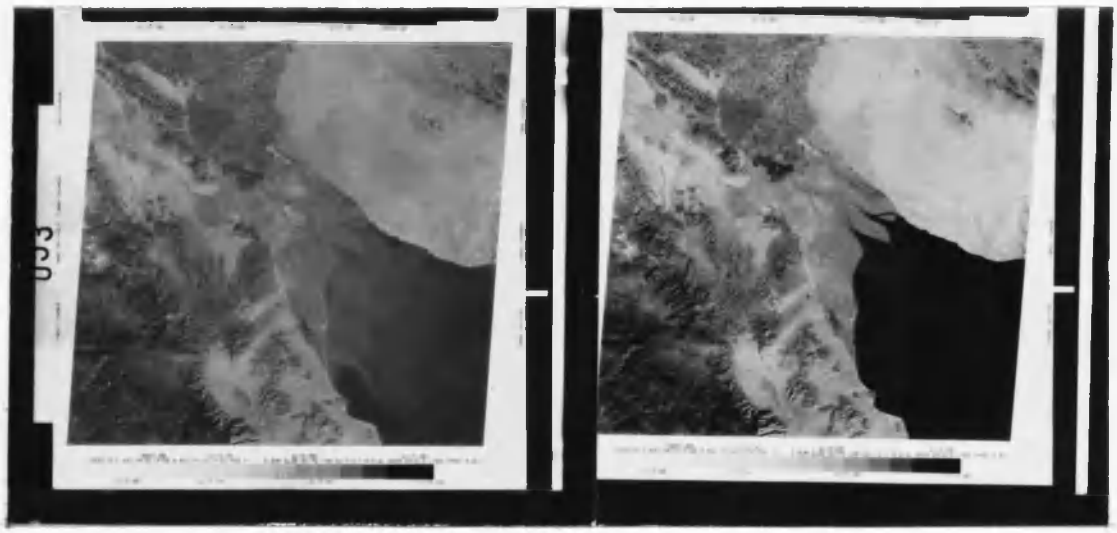

band 4 band 5

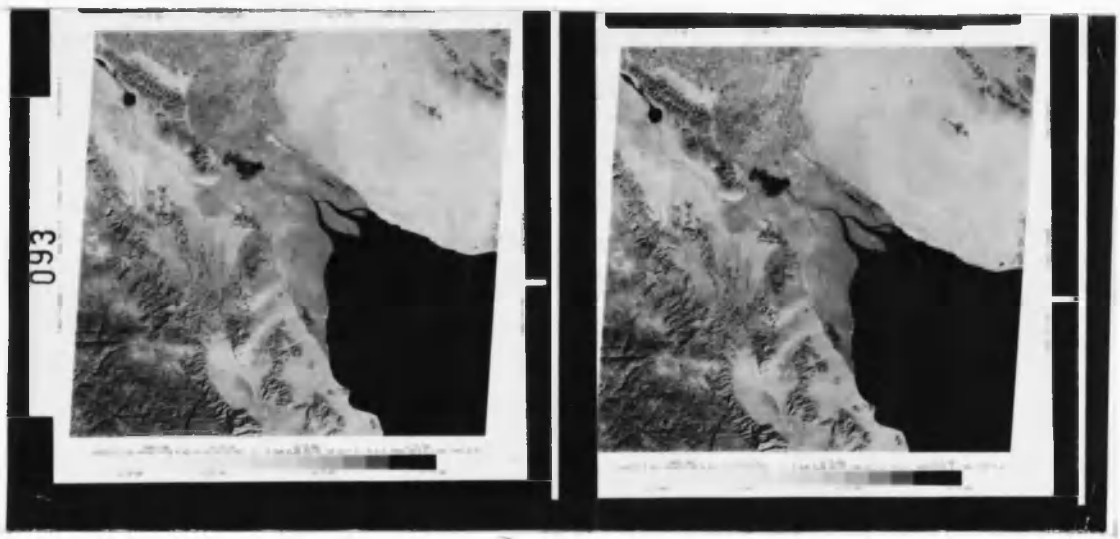

band 6 band 7

Figure 9. An example of ERTS-1 MSS winter imagery. -- Overpass corresponding to December 29, 1972.

4. The known properties of sea water (Duntley 1972, Lepley 1968) and the results of the Scripps Institute of Oceanography's "Fresnel II" survey in the Gulf (Austin 1972), were used as an aid to the interpretation of the ERTS-1 imagery under consideration.
5. The displacement of the light transmission peak from the blue-green region to the near infrared region in the four MSS channels may be utilized as a sounding device to get a three-dimensional picture of the distribution and flow of water masses at four depth intervals (Ross 1969).
6. In very turbid waters, the maximum light penetration is expected to be in the red band (Sverdrup, Johnson and Fleming 1963).

Using the known spectral properties of coastal sea water (Lepley 1968, Tyler and Smith 1970, Williams 1970), it is possible to predict the approximate thickness of the surface water layer in which or through which turbidity patterns are imaged in each of the four ERTS-1 MSS spectral bands. The depth of integration (penetration) is different for each of the four bands and is different for each degree of turbidity in the uppermost water layers.

The diagram shown in Figure 10 can be used to estimate relative depths seen by comparing the imagery of the four ERTS-1 bands. The use of this diagram was suggested by Lepley (1973) and is based on his experience in multispectral photography and radiometry over shallow water.

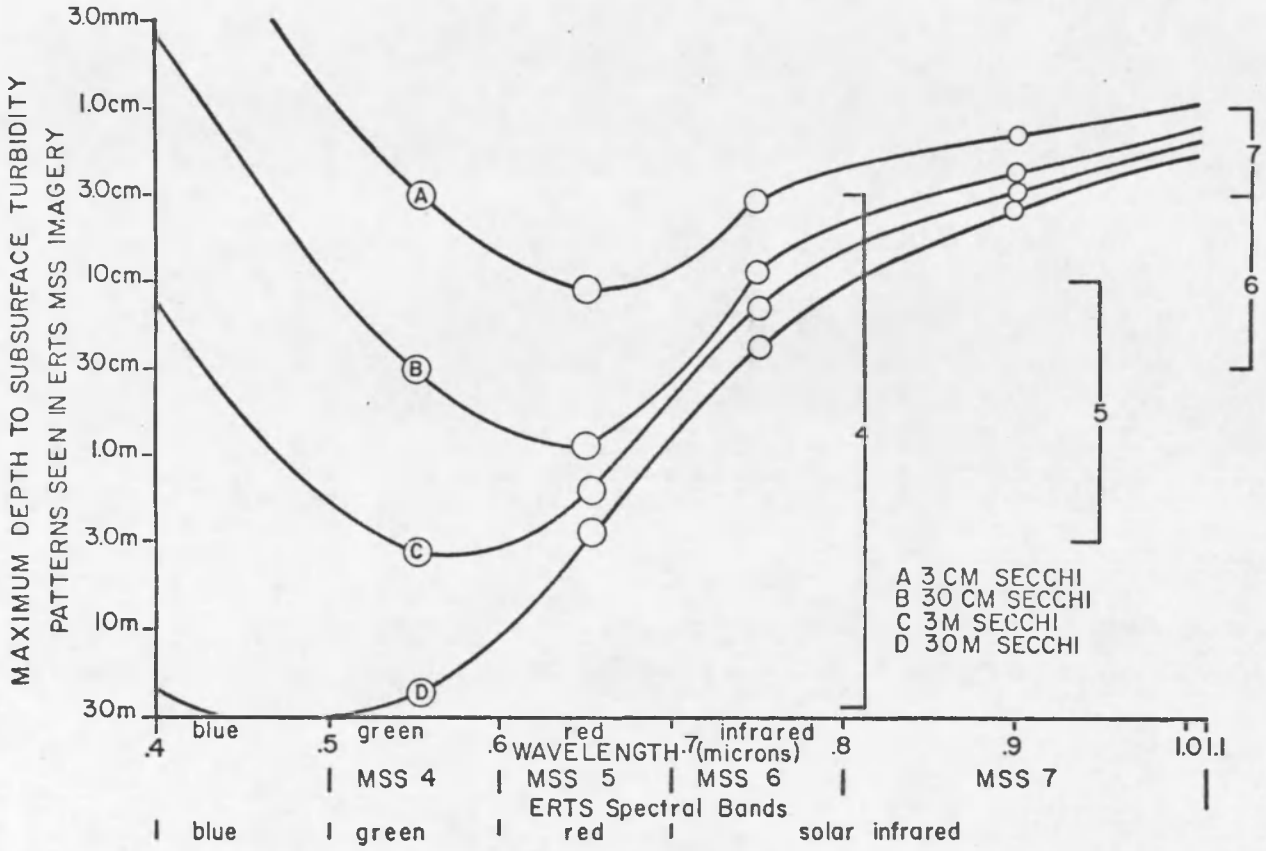

Figure 10. Penetrance of ERTS-1 MSS spectral bands, Northern Gulf of California. -- After Lepley (1973).

The use of this curve is as follows.

The selection of the appropriate curve A, B, C or D from Figure 10 according to the relative darkness of water in the four ERTS-1 MSS bands establishes the class of turbidity represented in the imagery. Curve D is selected when the water appears dark in all of the four channels. If the water appears dark in channels 5, 6 and 7, curve C should be selected. Selection of curve B is made when the water appears dark in channels 6 and 7. Curve A is chosen when the water appears dark only in band 7.

Once a curve is selected an approximate estimation of the depth of the turbidity patterns is possible. For example, if two superimposed patterns are seen in type C water on a band 5 image, but only one of these is seen on the band 7 image, then it is possible to conclude that band 7 shows the turbidity of the upper 15 cm and that band 5 shows the same pattern superimposed on a second pattern representing the 15 cm-150 cm depth interval.

In the analysis of the four different MSS bands, band 4 is expected to give information from a depth of three centimeters to a depth of 30 meters depending on the turbidity (the less the turbidity the greater the depth range of information). Band 5 (for the area of study) is expected to give information from three centimeters to three meters. The deepest penetration in very turbid waters can be expected to be in this band. In bands 6 and 7, the high absorptivity of the water predominates and the information from these bands represents the 3 to 30 centimeters and the 1 to 3 centimeters depth ranges respectively.

PHOTOANALYSIS TECHNIQUES

Visual Examination

The first step in the analysis of the selected imagery was a visual examination to delineate general marine features and at the same time to choose the best frames for further analysis. Due to the variation in water clarity in the northern Gulf, and the good resolution capability of the MSS, all four bands supplied a large amount of information when examined visually. Table 5 is a summary of the oceanographic features thus detected.

Analyzing the results of the visual examination one concludes that the examined imagery can be classified in two types according to the tonal contrast and resolution: (a) Summer-Fall imagery corresponds to the dry season in the area (May through October) and shows low contrast between the Northern Gulf Waters and the surrounding area. Yet for the water itself, the summer imagery gives the best information in turbidity levels, tidal pulsations, circulation patterns, wind effects over the surface layers, internal waves, and recurring plumes in the water. The early summer imagery in which the solar elevation was 60 degrees or more above the horizon shows that surface glitter or direct solar specular reflection from the water surface obliterated the subsurface turbidity patterns. However, these glitter patterns were found to be useful in themselves, in that bands of varying water roughness

Table 5. Catalog of oceanographic features of the northern Gulf of California from ERTS-1 MSS imagery.

Date	Frame ID	Band	Circulation Patterns	Tidal Stage	Glitter Patterns	Internal Waves	Suspended Sediments	Surface Currents	Sea-land Interface	Wind Effects	Upwelling Plumes
8/2/72	1015-17442	4									
		5					x				
		6		x			x	x	x		
		7		x			x	x	x		
8/24/72	1032-17391	4									
		5	x				x			x	
		6	x	x			x	x	x	x	
		7	x	x			x	x	x	x	
8/25/72	1033-17444	4									
		5					x				x
		6		x		x	x			x	x
		7		x		x	x		x	x	x
9/11/72	1050-17385	4									
		5	x								
		6	x	x							
		7	x	x							
9/11/72	1050-17392	4									
		5	x				x			x	
		6	x	x			x	x		x	
		7	x	x			x	x	x	x	
9/12/72	1091-17443	4									
		5	x				x			x	
		6	x	x			x	x	x	x	
		7	x	x			x	x	x	x	
9/12/72	1051-17450	4									
		5	x				x			x	
		6	x				x	x	x	x	
		7	x				x	x	x	x	
9/29/72	1068-17385	4									
		5					x	x			x
		6		x			x	x	x		x
		7		x			x		x		x
9/29/72	1068-17391	4									
		5									
		6		x					x		
		7		x					x		

Table 5, continued. -- Catalog of oceanographic features.

Date	Frame ID	Band	Circulation Patterns	Tidal Stage	Glitter Patterns	Internal Waves	Suspended Sediments	Surface Currents	Sea-land Interface	Wind Effects	Upwelling Plumes
9/30/72	1069-17443	4									x
		5	x				x				x
		6	x	x			x		x		x
		7	x	x			x		x		x
9/30/72	1069-17450	4									x
		5									x
		6		x					x		x
		7		x					x		x
11/4/72	1104-17393	4									
		5	x				x	x	x		x
		6		x			x	x	x		x
		7		x							
11/5/72	1105-17452	4									x
		5	x				x	x			x
		6		x			x		x		x
		7		x					x		
12/29/72	1159-17451	4					x				x
		5					x				x
		6		x					x		
		7		x					x		
12/29/72	1159-17454	4									
		5									
		6		x					x		
		7		x					x		
2/2/73	1194-17400	4									
		5					x				
		6		x					x		
		7		x					x		
2/3/73	1195-17452	4									
		5					x	x			
		6		x					x		
		7		x					x		
2/3/73	1195-17455	4									
		5									
		6		x					x		
		7		x					x		

Table 5, continued. -- Catalog of oceanographic features.

Date	Frame ID	Band	Circulation Patterns	Tidal Stage	Glitter Patterns	Internal Waves	Suspended Sediments	Surface Currents	Sea-land Interface	Wind Effects	Upwelling Plumes
3/10/73	1230-17400	4									
		5					x	x			
		6		x			x	x	x		
		7		x					x		
3/10/73	1230-17402	4									
		5					x				
		6		x					x		
		7		x					x		
3/11/73	1231-17454	4									
		5					x				
		6		x							
		7		x					x		
3/28/73	1248-17400	4									
		5					x	x			
		6		x			x		x		
		7		x					x		
3/28/73	1248-17408	4									
		5					x				
		6		x					x		
		7		x					x		
3/29/73	1249-17455	4									
		5					x	x			
		6		x					x		
		7		x					x		
3/29/73	1249-17461	4									
		5					x				
		6		x					x		
		7		x					x		
4/15/73	1266-17400	4						x			
		5				x	x	x			
		6		x	x	x	x		x		
		7		x	x	x			x		
4/15/73	1266-17402	4									
		5	x		x	x		x			
		6	x	x	x	x		x	x		
		7		x		x			x		

Table 5, continued. -- Catalog of oceanographic features.

Date	Frame ID	Band	Circulation Patterns	Tidal Stage	Glitter Patterns	Internal Waves	Suspended Sediments	Surface Currents	Sea-land Interface	Wind Effects	Upwelling Plumes
4/16/73	1267-17459	4									
		5					x	x			
		6		x			x	x	x		
		7		x					x		
4/16/73	1267-17461	4									
		5			x		x				
		6		x	x				x		
		7		x					x		
5/3/71	1284-17395	4									
		5			x		x	x			
		6		x	x			x	x		
		7		x	x				x		
8/3/73	1284-17402	4									
		5	x		x	x	x				
		6	x	x	x	x			x		
		7		x	x	x			x		
5/9/73	1285-17454	4									
		5									
		6		x					x		
		7		x					x		
5/4/73	1285-17460	4									
		5									
		6		x					x		
		7		x					x		
5/21/73	1302-17394	4									
		5			x	x	x	x			
		6	x	x	x	x		x	x		
		7	x	x	x	x			x		
5/21/73	1302-17401	4									
		5			x	x					
		6		x	x	x			x		
		7		x	x	x			x		
5/22/73	1303-17455	4									
		5	x		x		x	x			
		6	x	x	x		x	x	x		
		7		x	x				x		

Table 5, continued. -- Catalog of oceanographic features.

Date	Frame ID	Band	Circulation Patterns	Tidal Stage	Glitter Patterns	Internal Waves	Suspended Sediments	Surface Currents	Sea-land Interface	Wind Effects	Upwelling Plumes
5/22/73	1303-17455	4									
		5			x		x				
		6		x	x				x		
		7		x	x				x		
6/8/73	1320-17393	4									
		5			x				x		
		6		x	x				x		
		7		x	x				x		
6/8/73	1320-17395	4									
		5			x						x
		6		x	x	x			x		x
		7		x	x	x			x		
6/9/73	1321-17451	4									
		5			x		x				
		6		x	x				x		
		7		x	x				x		
6/9/73	1321-17454	4									
		5									
		6		x					x		
		7		x					x		
6/26/73	1338-17392	4									
		5									
		6		x					x		
		7		x					x		
6/26/73	1338-17394	4									
		5			x						
		6		x	x	x			x		
		7		x	x	x			x		
6/27/73	1339-17450	4									
		5			x		x	x			
		6		x	x		x	x	x		
		7		x	x		x		x		
6/27/73	1339-17453	4									
		5	x		x		x				
		6	x	x	x		x		x		
		7	x	x	x		x		x		

Table 5, continued. -- Catalog of oceanographic features.

Date	Frame ID	Band	Circulation Patterns	Tidal Stage	Glitter Patterns	Internal Waves	Suspended Sediments	Surface Currents	Sea-land Interface	Wind Effects	Upwelling Plumes
7/14/73	1356-17390	4									
		5			x		x	x			
		6		x	x	x		x	x		
		7		x	x	x			x		
7/14/73	1356-17396	4									
		5			x	x					
		6		x	x	x			x		
		7		x	x	x			x		
7/15/73	1357-17445	4									
		5			x		x	x			
		6		x	x		x	x	x		
		7		x	x		x		x		
7/15/73	1357-17451	4									
		5	x		x		x				
		6	x	x	x				x		x
		7		x	x				x		x

would reconstitute, on the sea surface, an image of subsurface oceanographic phenomena which become apparent in the satellite imagery. Figure 11 shows an example of summer imagery. (b) Winter-Spring imagery corresponds to the rainy season in the area (November through April) and exhibits good contrast between the gulf waters and the surrounding land, but in the water itself the contrast is attenuated and oceanographic information is given mainly by band number 5. The water in bands 6 and 7 is shown with the same level of density. This means that the surface waters during these months are very homogeneous with a low level of turbidity. Figure 9 shows a set of data corresponding to this kind of imagery.

The reasons for the seasonal differences evident in the imagery discussed above are primarily (a) changes in sun elevation and (b) changes in the weather conditions. Sun elevation as well as weather changes affect the reflectivity conditions. During the summer when the sun reaches its higher elevations in the area and the dryness of the land area is at a maximum, the observed contrast between the exposed land and the water reaches its minimum value (NASA 1972). The opposite happens when the sun reaches its lowest elevations and the land area is wet during the winter season.

Density Slicing Method

This technique consists in converting electronically and instantaneously the shades of gray in an image or scene into a wide spectrum of colors (density levels of a photographic transparency and converted into colors) so areas of special interest may be shown in detail.

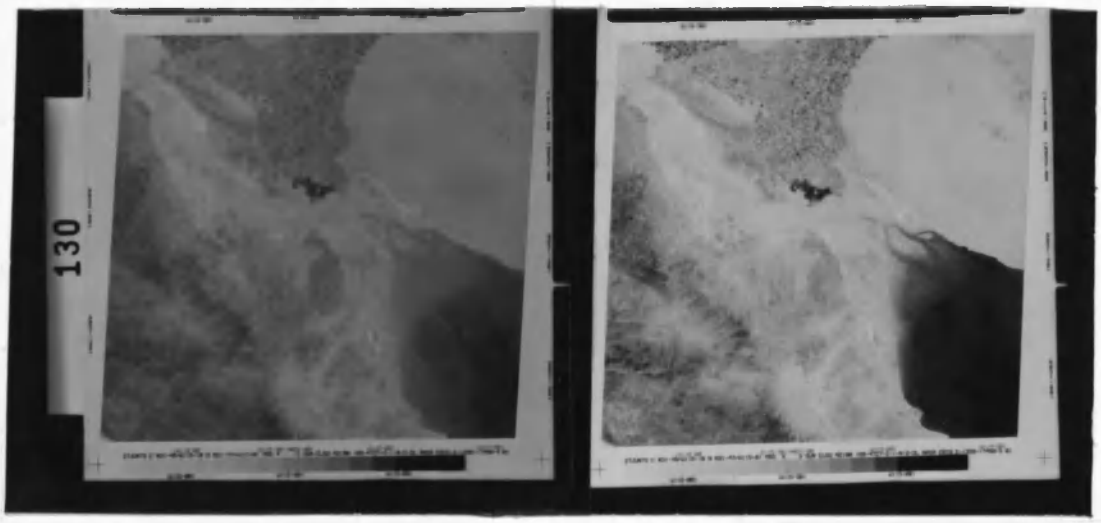

band 4 band 5

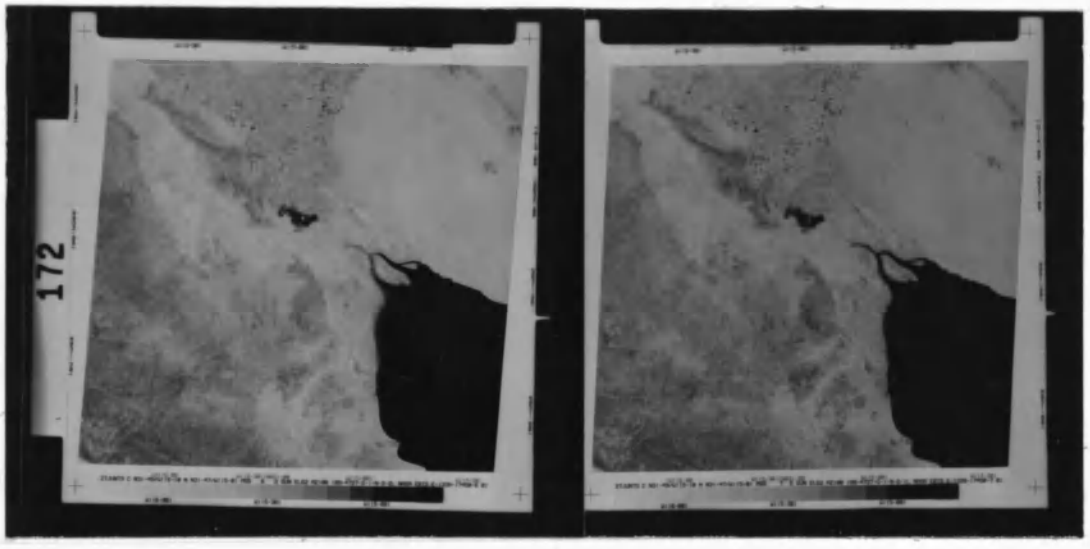

band 6 band 7

Figure 11. An example of ERTS-1 MSS summer imagery. -- Overpass corresponding to June 27, 1973.

The equipment used for this project was a Spatial Data Model 704/8 of the Arizona Regional Ecological Test Site. This system uses a black and white video camera to produce a standard television signal. An on-line digital video processor analyzes the shades of gray in the television signal. The gray shades are classified into one of eight categories. A different color is assigned to each category; the appropriate color television signal for the color is generated by the digital processor. The final result is a complete color signal suitable for operation of a color monitor unit. The colors on the monitor correspond to the shades of gray in the original black and white picture. For this particular case the color contours indicate relative gray tone values in the ERTS-1 imagery. The color sequence runs from white at the off-scale portion of the bright end of the gray scale to black at the off-scale portion of the dark end, as follows: white; dark blue; green; yellow; brown; red; magenta; black. As a general but not absolute rule, the sequence from white to black corresponds with a range from very turbid to clear water.

August 24, 1972, Imagery

Figure 12 shows the video-densitometer enhanced imagery corresponding to this date (orbits 1032 and 1033). The tide was at mid-stage and rising. Northwest-flowing tides can be seen as spears of water (blue color) intruding into estuaries in band 6 of orbit 1033. Superposed over the northwest tidal streamers are a surface turbidity sheet running in a north-south direction (green contour in band 7 of orbit 1033). This sheet appears to emerge from the north shore of the

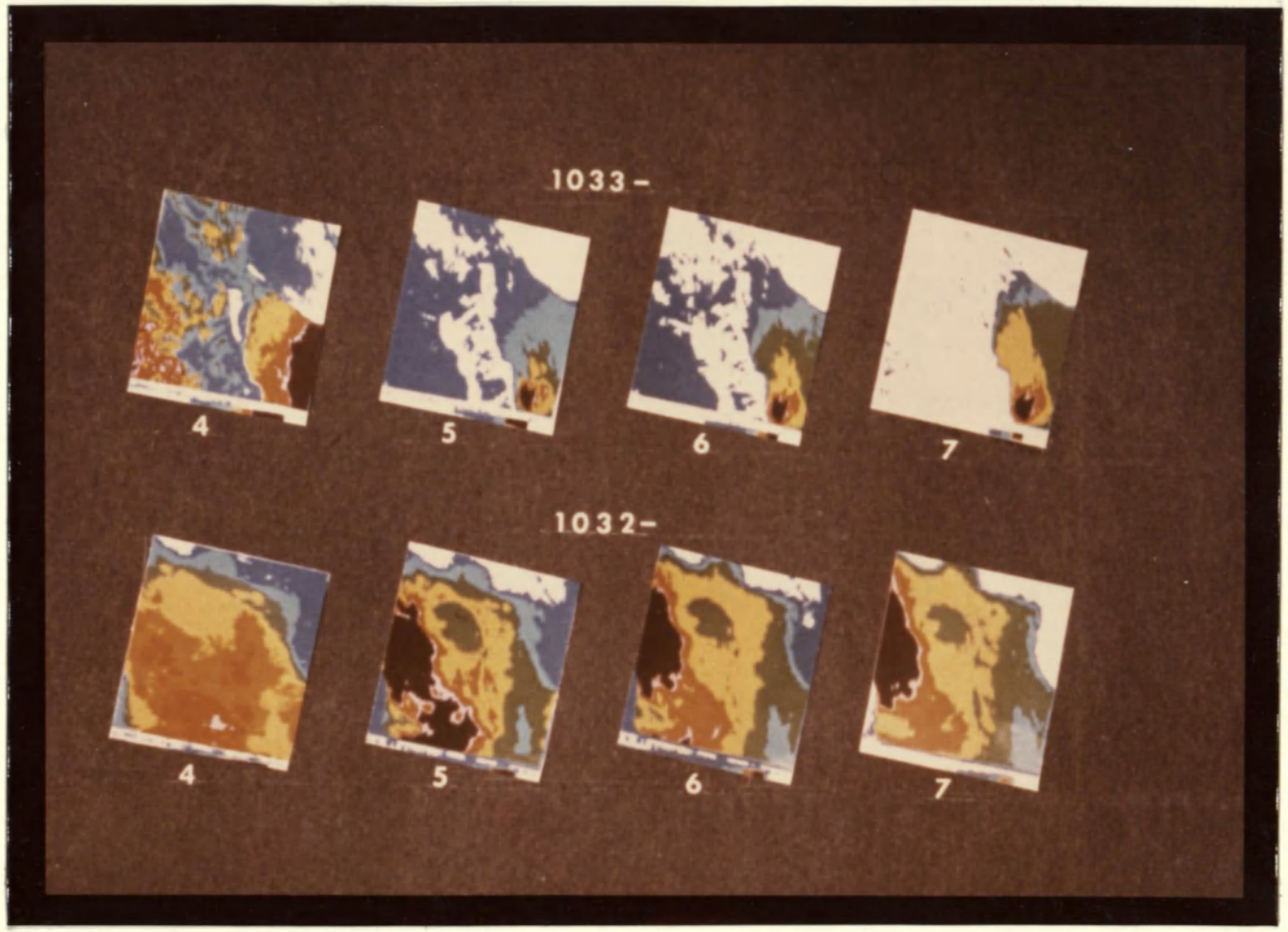

Figure 12. Video-densitometer enhanced imagery. -- Overpass corresponding to August 24, 1972.

gulf and move in a southerly direction, indicating a wind blowing from north to south which pulled up turbid water in the north and caused a downwelling of the clearer (black) surface layers to the south. Cloud positions coincide with the western edge of this north-south surface turbidity layer. This cloud streamer is presumed to mark the western edge of the south-moving air mass.

In orbit 1032 a gyre, best shown by longer wavelengths, seems to be indicated by a turbidity pattern of rotary surface currents moving in a counterclockwise direction around an eye at $31^{o}00'N$, $114^{o}10'W$. The gyre has a diameter of approximately 40 nautical miles (green in bands 5, 6 and 7).

Color Additive Enhancement Method

Although significant information can be extracted from the imagery by sequential or comparative interpretation of each of the four frames comprising the MSS set, a significantly more productive analysis can be made by simultaneous additive color viewing.

The principles of additive color viewing of multispectral imagery are quite straightforward. The basic concept is simply that a color composite image can be produced when one optically projects positive photo transparencies of images which are:

1. Taken in different parts of the spectrum.
2. Projected through different colored filters.
3. Superimposed one upon the other in accurate registration.

Figure 13 shows a color composite image obtained with the I^2S miniadcol multispectral viewer of the Arizona Regional Ecological Test Site. This color enhanced image was obtained using the simple arrangement of additive color viewing of the green, red and infrared "black and white" multispectral positives projected through blue, green, and red filters respectively (false color combination). The imagery corresponded to the November 5, 1972, satellite overpass.

Analyzing this color-additive enhanced imagery, one finds that for this particular area not much more data can be extracted from it with respect to visual examination since most of the information about the gulf waters is contained in band 5. Nevertheless, the following interpretation was made. A mass of clear water (dark blue), a possible upwelling near the port of San Felipe, is identified. The difference in turbidity levels of the waters near Isla Montague (northwestern part of the area) is shown by different tonalities of blue. The dark blue color seen in the lower right corner of the imagery represents deeper waters. This false color combination technique is very useful for land vegetation mapping purposes. The red tones in the false color image under consideration represent vegetated areas.

Figure 14 shows the same imagery processed through a reversed color additive combination with a red filter assigned to the green band, a green filter assigned to the red band, and a blue filter assigned to the IR band. This filter combination is more useful for the study of oceanographic features than the other color combination. The turbidity streamers are much better delineated as are the tidal pulsations.

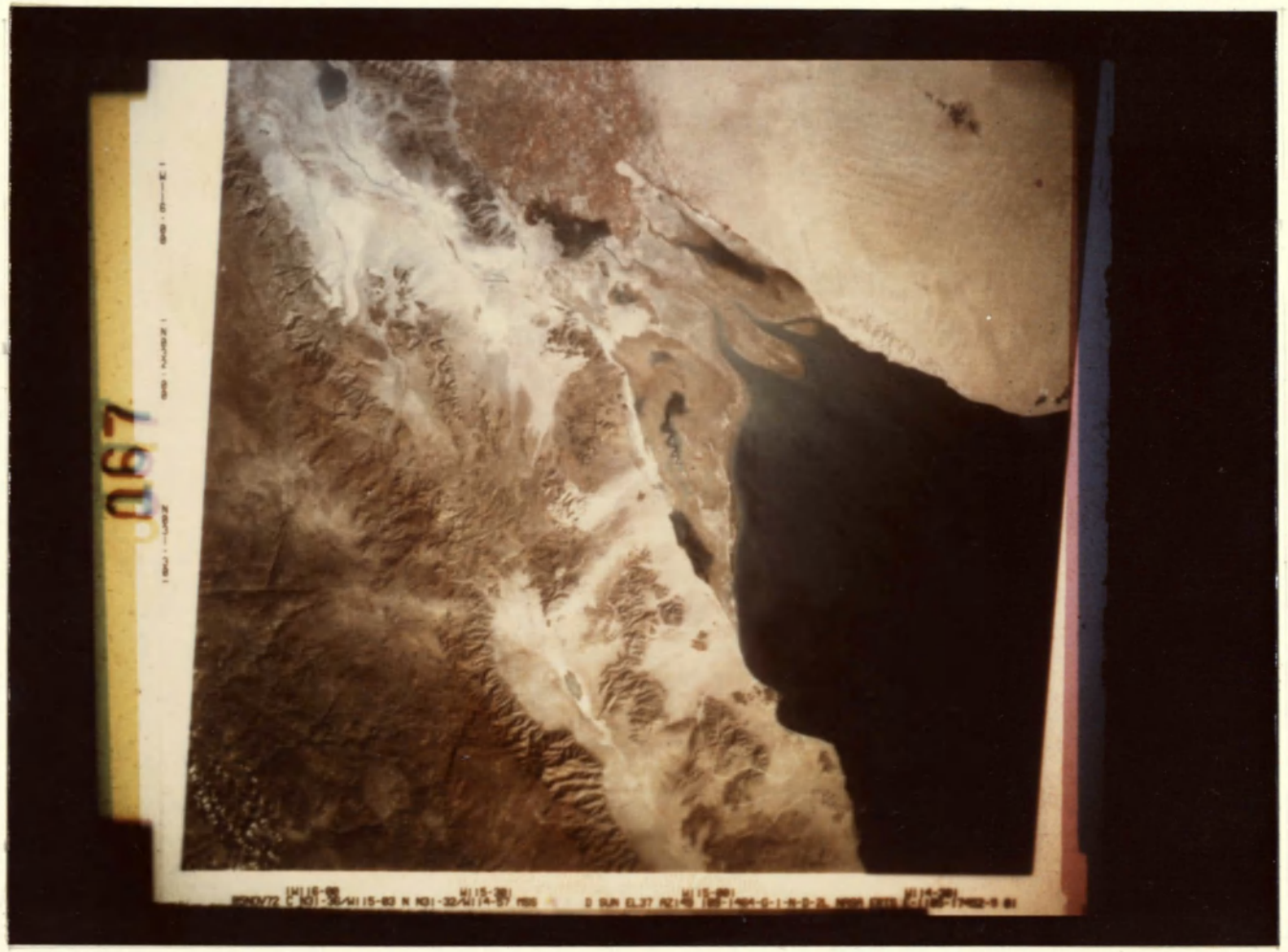

Figure 13. Color addition enhanced imagery (false color). -- Satellite overpass corresponding to November 5, 1972.

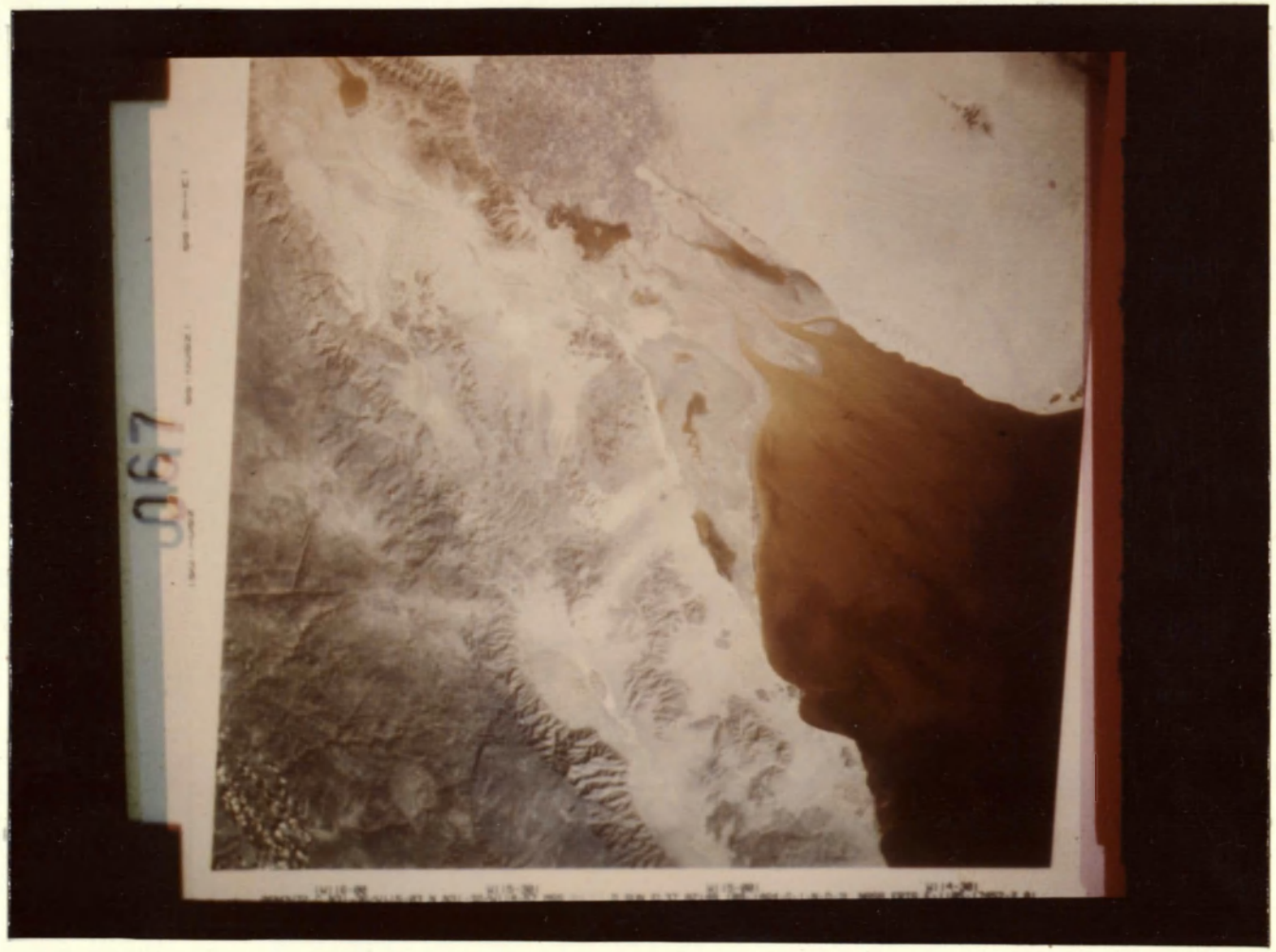

Figure 14. Reversed color addition technique. -- ERTS-1 imagery corresponding to the November 5, 1972, overpass.

Reprocessing of the Imagery Method

This method of analysis consists of rephotographing the ERTS-1 imagery to provide a higher contrast and a better gray scale range. This technique proved to be the most valuable one in the oceanographic analysis of the ERTS-1 imagery for the area. Figure 15 shows an example of the kind of data obtained using this technique. The contrast among the different features on land is lost completely (white areas), but the contrast in the water itself is increased enormously. This imagery corresponds to the satellite overpass of September 11, 1972.

A turbidity front and its counterclockwise rotation can be delineated to a greater degree using this technique. In band 7 the clouds at the edge of the gyre are quite distinguishable due to the high contrast between the clouds and the surrounding gray water areas. Using the sounding properties of the MSS imagery and curve B of Figure 10, one can deduct that vertically the turbidity extends from a depth of about 2 meters up to approximately three millimeters below the water surface.

The results of the data analysis will be discussed later using mainly imagery processed by this technique.

Data Analysis with Ground Truth

In order to correlate what is actually seen by the MSS from 490 nautical miles of altitude with the real phenomena, another kind of analysis of the ERTS-1 imagery was undertaken. This analysis used ground truth data gathered by the research ship, "Adventyr," operated at the time by The University of Arizona. The data was used to construct a working model that related the spectral reflectance of the area under

band 4 band 5

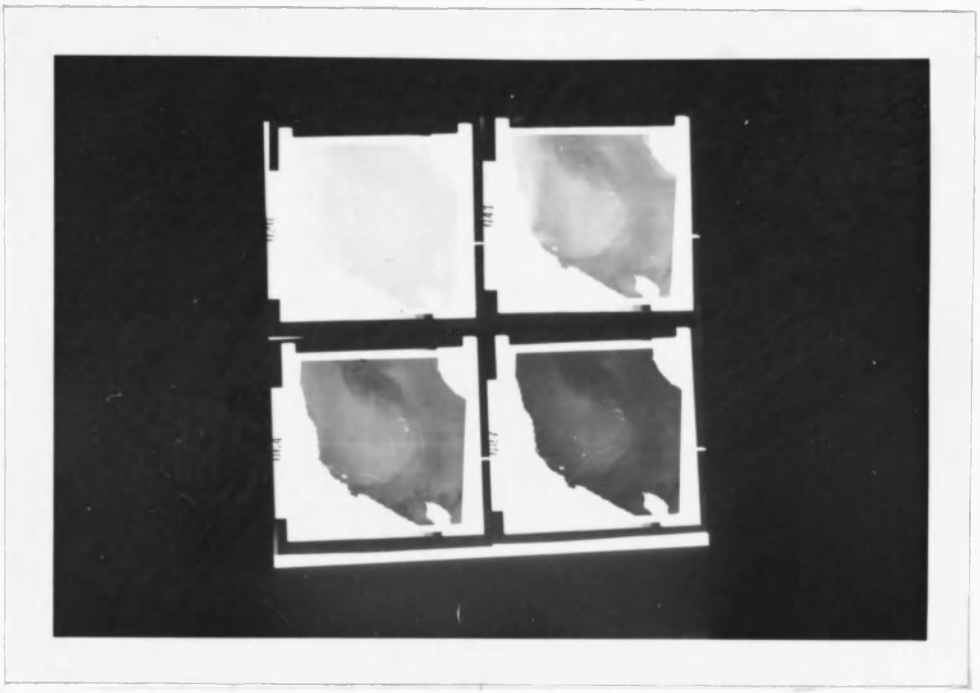

band 6 band 7

Figure 15. Reprocessing of a MSS imagery quadrant to show the enhancement of water features. -- Overpass corresponding to September 11, 1972.

study, as sensed by the MSS, with the real reflectance as seen from two meters.

The surface truth data used in the image interpretation were mainly spectroradiometric readings, some of them taken by this writer, during the oceanographic cruises of January, March, April, May and June of 1973 (Hendrickson 1973). ERTS- matched reflectance spectra from 2 meters above the water surface was collected using an Exotech four-channel radiometer made available by the Arizona Regional Ecological Test Site (ARETS) program. Appendix A shows the spectroradiometric data used in the analysis, and Figure 16 shows the oceanographic stations at which the data was obtained. Figure 17A, 17B, and 17C shows this data plotted as un-normalized reflectance spectra. Two readings were taken with each of the channels--one reading of downwelling incident radiation over a field of view of 160^{o} through a diffusing plate and the other of upwelling scene radiance over a 15^{o} field of view. The ratios of these sets of readings in each of the channels were plotted without any attempt to normalize to 100 percent reflectivity.

The plotted data was then identified with corresponding turbidimeter, secchi disk, ocular, and other observations summarized in Table 6. This table was constructed to show the classes of water to which the spectral curves correspond. Two assumptions were made in the analysis of the ERTS imagery and surface spectroradiometric data:

1. The transparency of clear water decreases monotonically with an increase in wavelength of the four MSS bands.

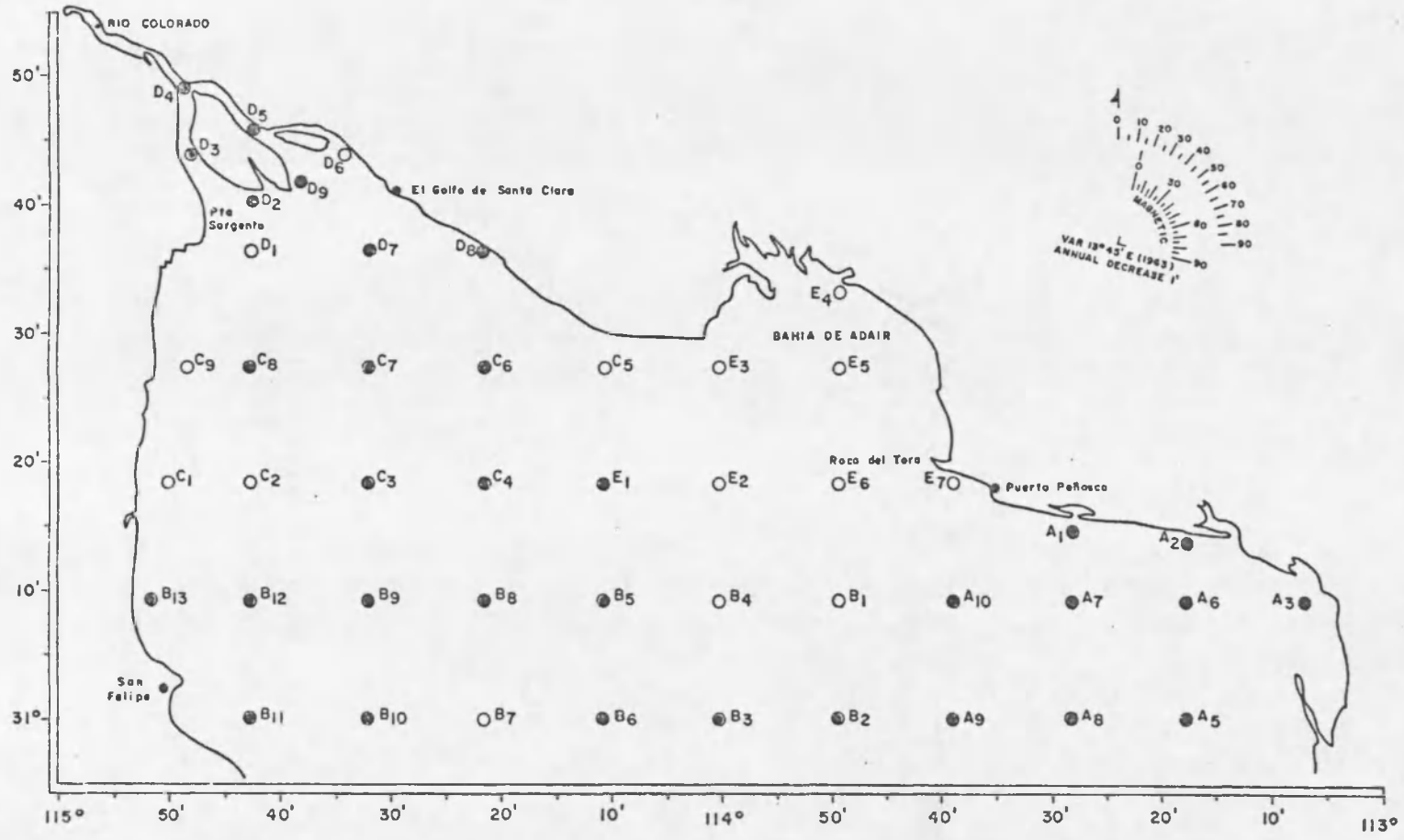

Figure 16. Oceanographic stations at which spectroradiometric data was obtained (dark circles).

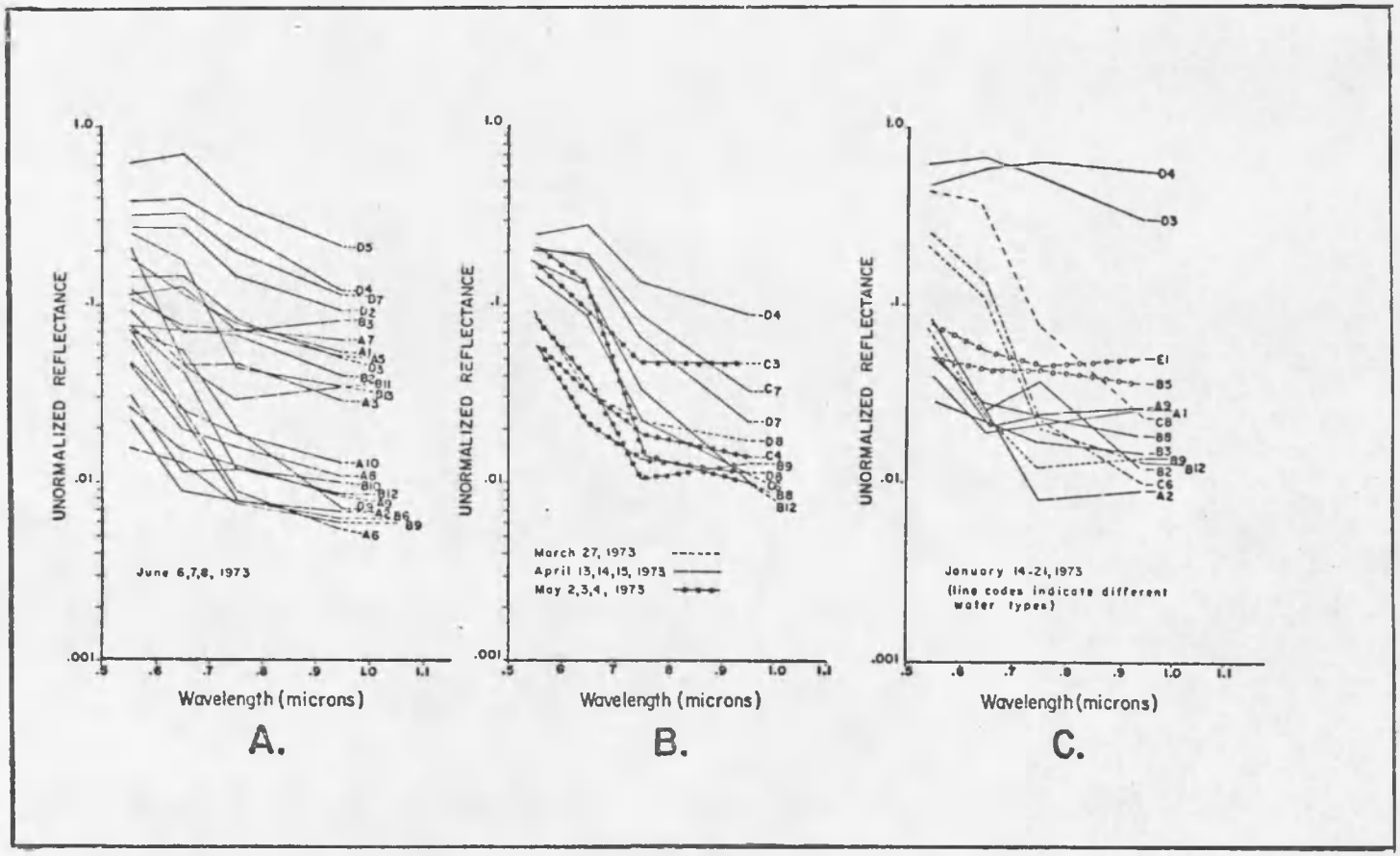

Figure 17. ERTS-1-matched reflectance spectra from oceanographic stations, Northern Gulf of California.

Table 6. Identification of water types in the Northern Gulf of California from spectroradiometric and surface truth data.

Stations	Surface Observations
D2, D3, D4, D5, D6, D7, D9	Water very turbid. Depths less than 4 meters. Secchi disk readings from .25 to .80 meters.
C3, C6, C7, C8, D8	Water semiturbid high plankton content. Secchi disk readings from 1 to 4 meters.
A1, A2, A8, A9, A10, B2, B3, B5, B6, B8, C4	Clear water. Secchi disk readings greater than 5 meters.
B9, B10, B11, B12, B13	Clear water over turbid water. Secchi disk readings vary from 2 to 5 meters.

2. The head of the gulf is usually formed by a wedge of clearer water which thins toward the Colorado River estuary and overlies at least one layer of very turbid water.

The imagery of the ERTS-1 overpass corresponding to the January, 1973, surface truth cruise consisted mostly of clouds, but fortunately, the previous December 29 ERTS overpass corresponded to an analogous tidal situation.

The spectroradiometric data (Figure 17) show a tendency to cluster according to (a) depth of clear water over the underlying turbid layers, (b) the amount of suspended matter in clear water and (c) clarity of the surface layer.

Other surface truth data used in the image interpretation, included secchi disk measurements, turbidity, wind velocity and direction, and temperature profiles. This data is described in Hendrickson (1973) sections III-2 and III-7.

The spectral reflectance data taken during all of the surface truth measurement cruises, when plotted as reflectance in one spectral band versus reflectance in another, were found to cluster especially well when band 4 was plotted against band 6 as shown in Figure 18A and when band 5 was plotted against band 7 as shown in Figure 18B. Two aspects of these plots are significant. The clusters representing the bodies of waters that were considered likely to contain high biological content are located in the areas corresponding to those of intermediate turbidity. It is also important to note that the reflectance spectra of layers of relatively clear water overlying turbid water are different from those of unlayered mixed water of any particular turbidity. This result implies that, with remotely sensed spectral data, mixed water bodies can be separated from stably laminated bodies of water. The analyses of this spectral data, coupled with sub-surface measurements of secchi disk and turbidimeter readings taken by the "Adventyr" and by Scripps Institute of Oceanography (Austin 1972) were indispensable in the interpretation of the multispectral satellite data.

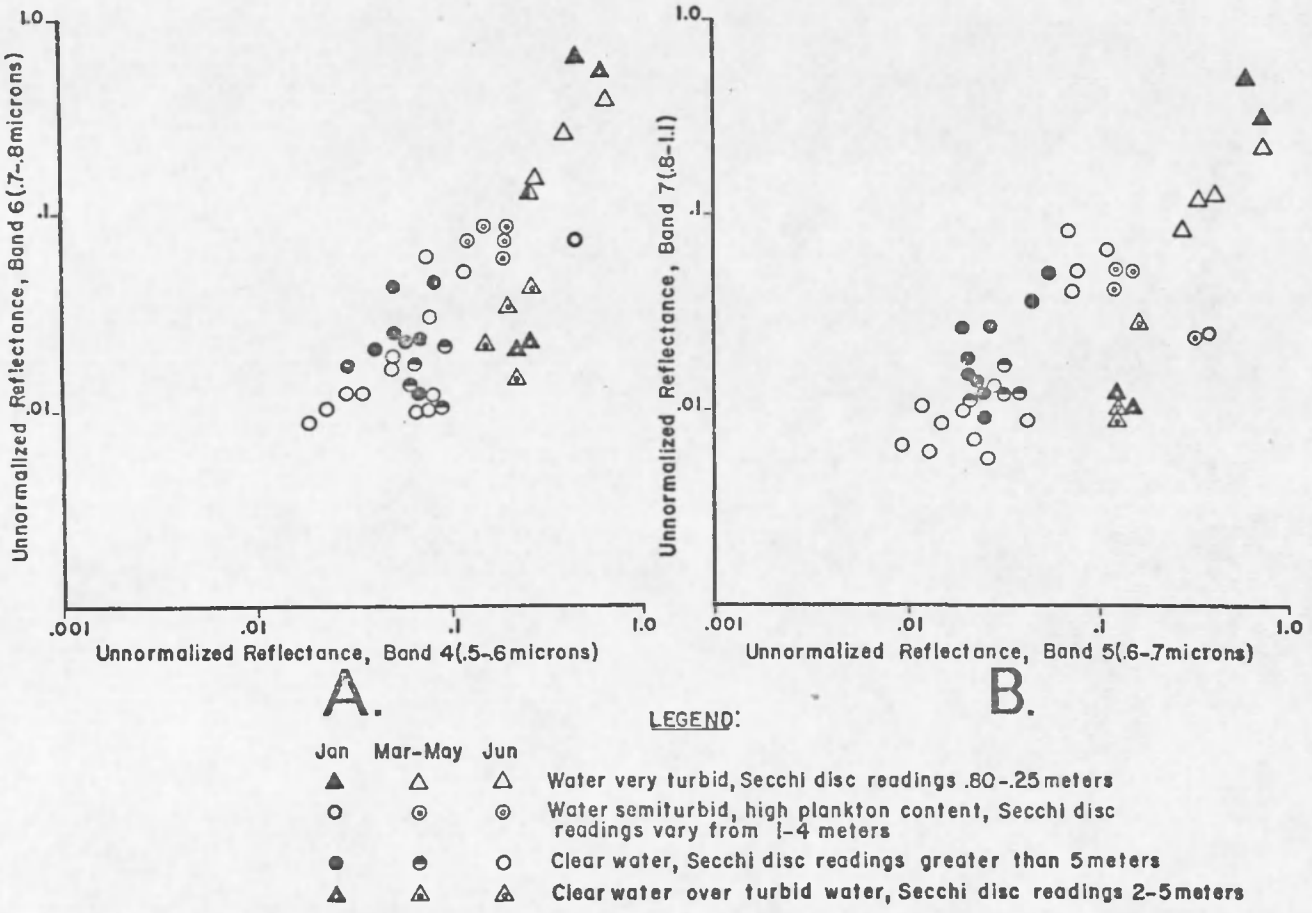

Figure 18. Band plots of ERTS-matched reflectance spectra from oceanographic stations, Northern Gulf of California.

RESULTS OF DATA ANALYSIS

Circulation Patterns

It was possible to study gross circulation in the surface layers of the Northern Gulf of California because suspended sediment acts as a natural tracer. Counterclockwise gyres were detected especially in the summer imagery. Figure 19A and 19B shows two gyres present on August 24th and September 11th, 1972. These gyres are all cyclonic, converging upon a vortex. These types of counterclockwise circulation patterns in the Northern Gulf of California have been reported before by Thompson (1969b). He pointed out that, in comparable situations of semi-enclosed long bays like the North Sea and the Adriatic Sea, the rotary tidal circulation is also counterclockwise, which is consistent with theoretical models (Defant 1958) in which the surface waters flow in a north-south direction. This north-south flow is indeed observed in the imagery under consideration. The problem is that, according to theory (Emilsson 1972), the circulation for areas like this would be controlled by the thermohaline conditions (with the haline conditions predominating) and should be in a south to north direction. Considering the theory for long-narrow bays like the area of study, in which the evaporation exceeds the precipitation one finds that the salinity is determined by the balance between the fresh water inflow (through the sea-atmosphere and sea-land boundaries) and the water exchange with the exterior sea. In a long

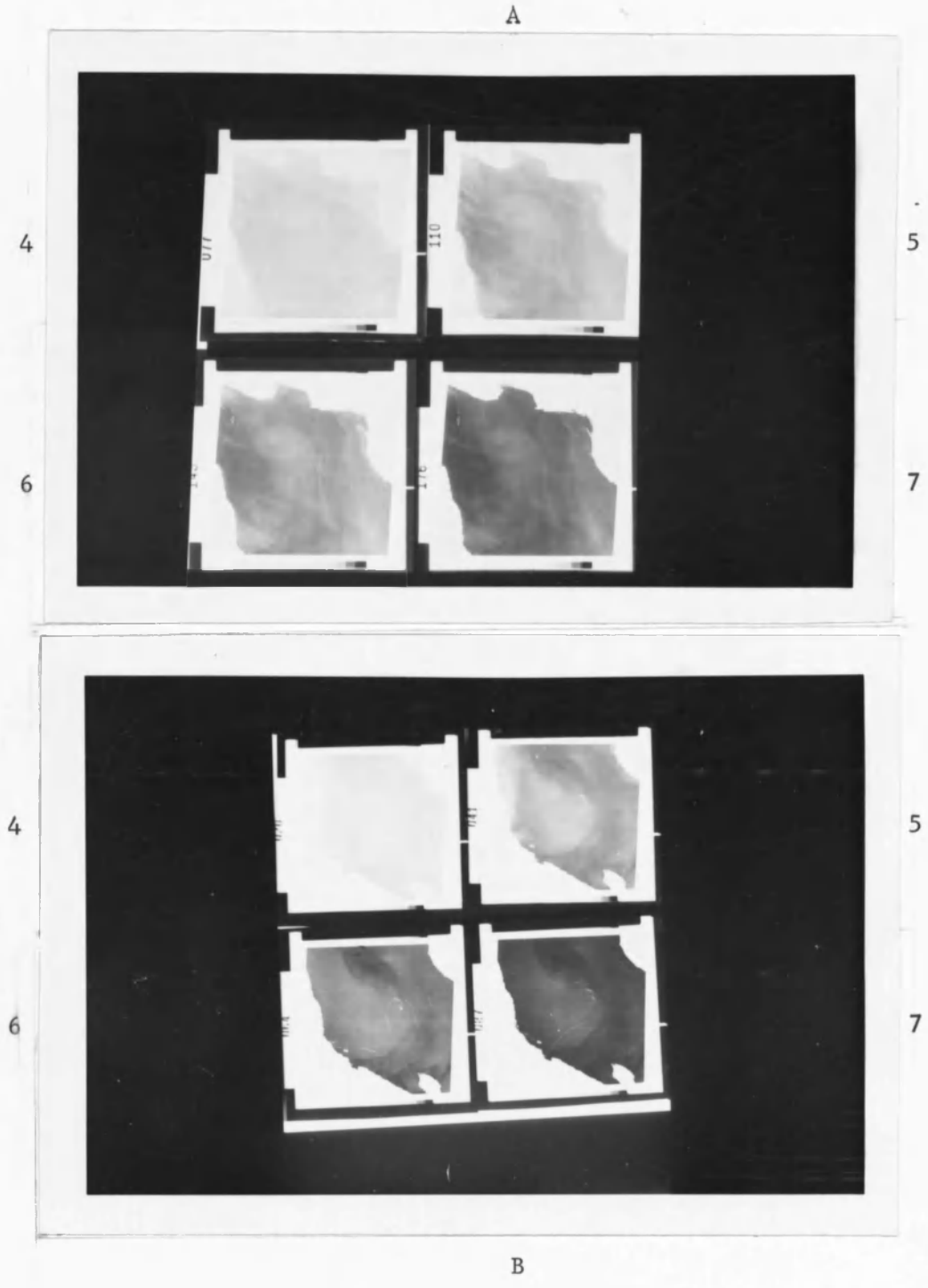

Figure 19. Examples of counterclockwise turbidity gyres. -- (A) Imagery from August 24, 1972. (B) Imagery from September 11, 1972.

term, an equilibrium is reached, so that the amount of salt entering from the exterior sea is equal to the amount of salt leaving the interior sea.

The salt conservation requires that:

$$F_E S_E = F_L S_L$$

where

F_E = Mass of water entering the area.

S_E = Salinity of the mass of water entering the area.

F_L = Mass of water leaving the area.

S_L = Salinity of the mass of water leaving the area.

Since the mass of water in the region must be constant, it follows that:

$$F_L = F_E + R - (E - P)$$

where

R = Fresh water inflow through the sea-land interface.

E = evaporation.

P = precipitation.

Combining both equations F_E is found to be:

$$F_E = \frac{[R - (E - P)]S_L}{S_E - S_L} .$$

This equation gives an idea of the circulation which can be expected in semi-enclosed areas when the hydrological regime and the salinity of waters entering and leaving the region are known.

For the Northern Gulf of California (during the summer) R is negligible and the evaporation exceeds the precipitation (Alvarez-Borrego, Nishikawa-Kinomura and Florez-Munoz 1974; Green 1969) so R - (E - P) is negative and this requires that S_L be greater than S_E (Emilsson 1972). In adjacent regions in which the temperature of surface waters is usually about the same, the difference in density (ultimately responsible for circulation) depends essentially on the salinity.

In the first analysis of the area, and taking into consideration a negative hydrological balance, one finds that the saltier water is the water leaving the area. Because this water is heavier, it should be close to the bottom and the surface circulation should be in a south-north direction as shown in Figure 20A, but this is not the case according to ERTS-1 imagery. A reason for this was found by checking the surface temperatures and salinities (Hendrickson 1973) of the area during the summer of 1972. One finds that there are as many as three degrees centigrades of difference between the delta stations and the sea stations. In another case, the temperatures of adjacent regions were different and the density was influenced to a greater extent by the temperature. The density of the surface waters in the delta area was reduced in such a way that the waters at the northern end of the gulf could not sink any more than expected in Figure 20A if the circulation were controlled only by salinity.

It follows that one would expect the surface salinity also to be greater in the delta area stations than in the sea stations and this evidently occurs (Alvarez-Borrego et al. 1974, Hendrickson 1973). The

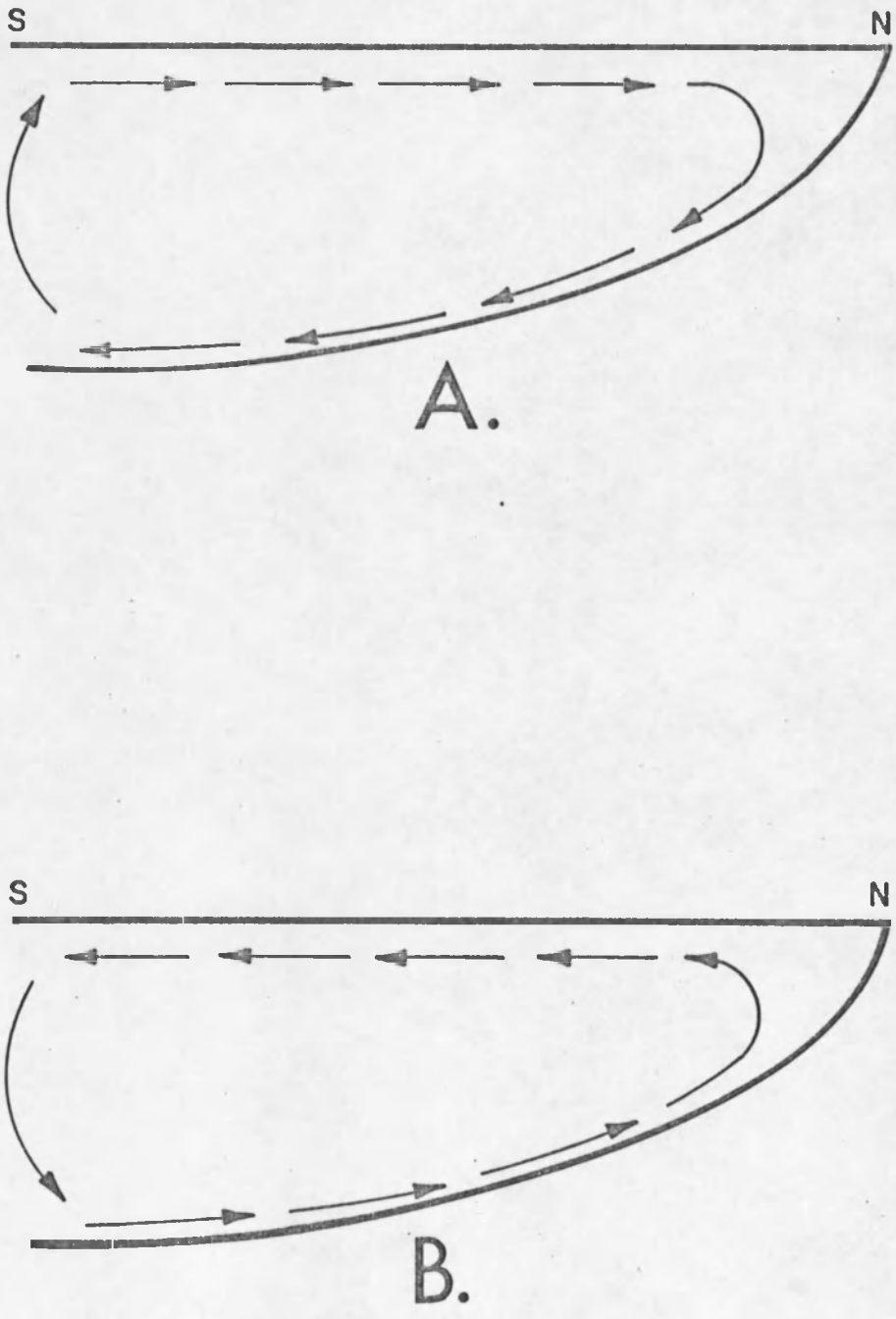

Figure 20. Summer circulation, Northern Gulf of California. -- (A) Assumed haline dominated circulation; (B) ERTS-1 suggested thermal dominated circulation.

density of this water is affected more by temperature than by salinity and therefore tends to flow in the direction of lower surface temperature waters which are found in the sea stations south of the delta. In this area the south-flowing water cools, increases its density and sinks. The constancy of the water masses in the region requires a net circulation in a north-south direction in the surface and opposite circulation near the bottom forming a convection cell (Figure 20B). This is consistent with the author's interpretation of the ERTS-1 data.

In the winter (November through March) the surface truth data shows that the surface temperature in the delta area is 5°C colder than the water in the center of the upper gulf. The surface salinity is also greater in the delta stations by .5 parts per thousand. The data show that even in the winter (when some rain was reported) the negative hydrological balance still persists and the general circulation is more of the thermo-haline type with the saltier and colder bottom waters (those which sink at the head of the gulf) being the leaving waters and the less salty and hotter surface waters being the entering waters. In this manner, a convection cell is formed (Figure 21). Since the surface circulation is now in a south to north direction, the entering water coming from deeper parts at the center of the upper gulf is expected to have a very small amount of suspended sediments. This would make difficult the analysis of circulation patterns in the winter imagery since the natural tracer (suspended sediments) used for the summer circulation patterns analysis is now lacking. In fact, this was observed during the analysis of winter imagery, one example of which is Figure 9 where bands

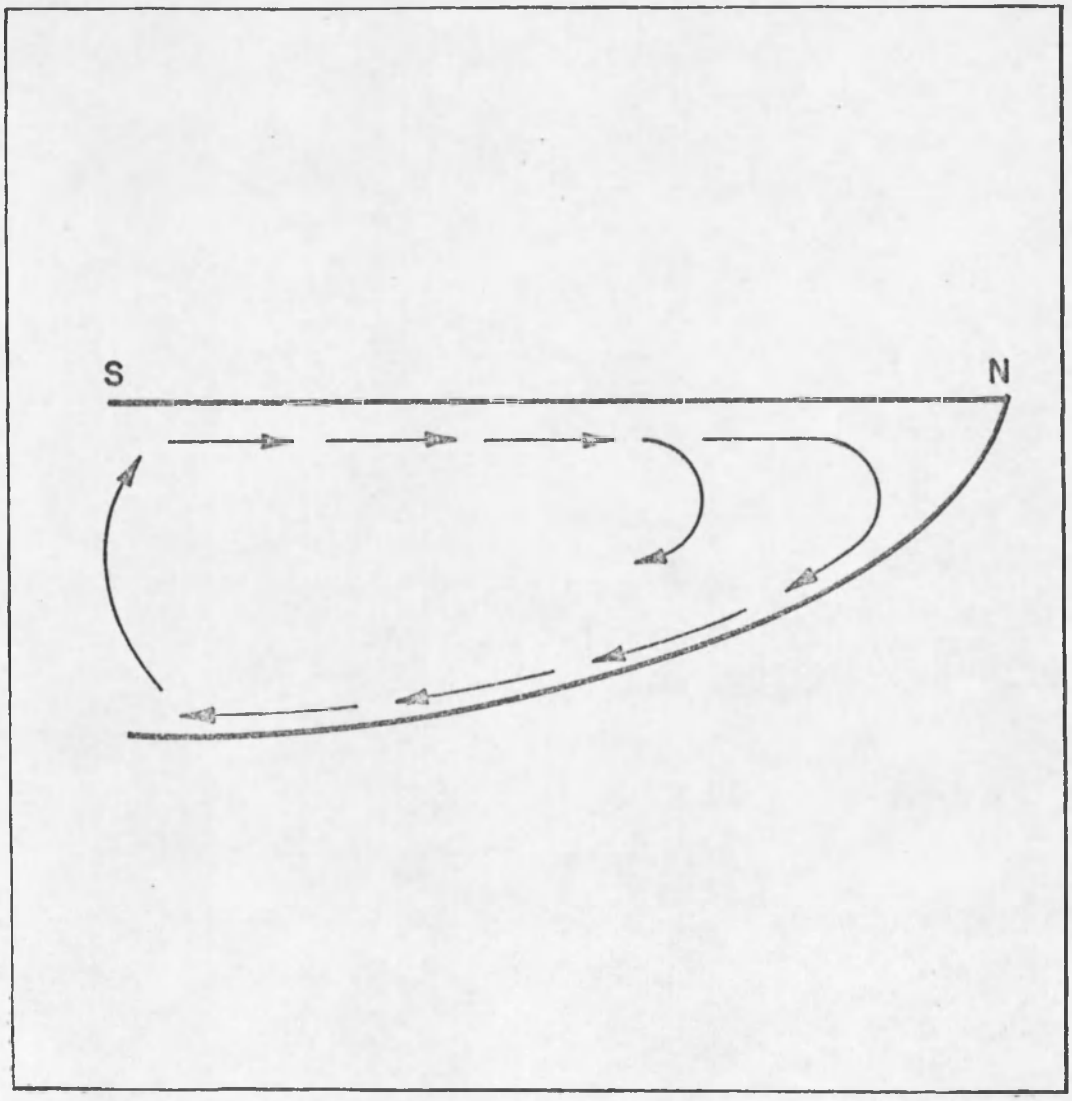

Figure 21. ERTS-1 suggested thermohaline winter circulation model for the Northern Gulf of California.

6 and 7 show that the surface waters are not turbid (uniform gray density).

Upwelling Plumes

Lepley (1973) proposed a circulation model based on thermal convection and the Coriolis effect to obtain an idealized circulation model that closely resembles what is actually seen in ERTS-1 summer imagery (north to south surface circulation and counterclockwise gyres). According to this model, the principal heat source for this thermal influenced circulation is the well-flushed shallow tidal waters of the Colorado River delta which in time are heated by conduction from the nearby Gran Desierto. The surface circulation is north to south and the bottom circulation is south to north. Thus a convection cell is formed. The Coriolis force deflects the surface stream to the right as it moves down into the main area of the upper center gulf, and a major counterclockwise gyre is formed around a center of downwelling, cooled water. Figure 22A represents the surface flow in summer according to the model. The longitudinal flow is the same as shown in Figure 20B. The transverse flow is shown by Figure 22C. The point of downwelling in the sectional diagram coincides with the center of the gyre in the main diagram. Figure 22B represents compensatory subsurface movements in accord with Coriolis effect and physical oceanographic theory (Defant 1958). This pattern would produce areas of upwelling at points along the coast with offshore drift to complete the cell. The analysis of the summer imagery, in fact, showed plumes of darker (clearer) water which

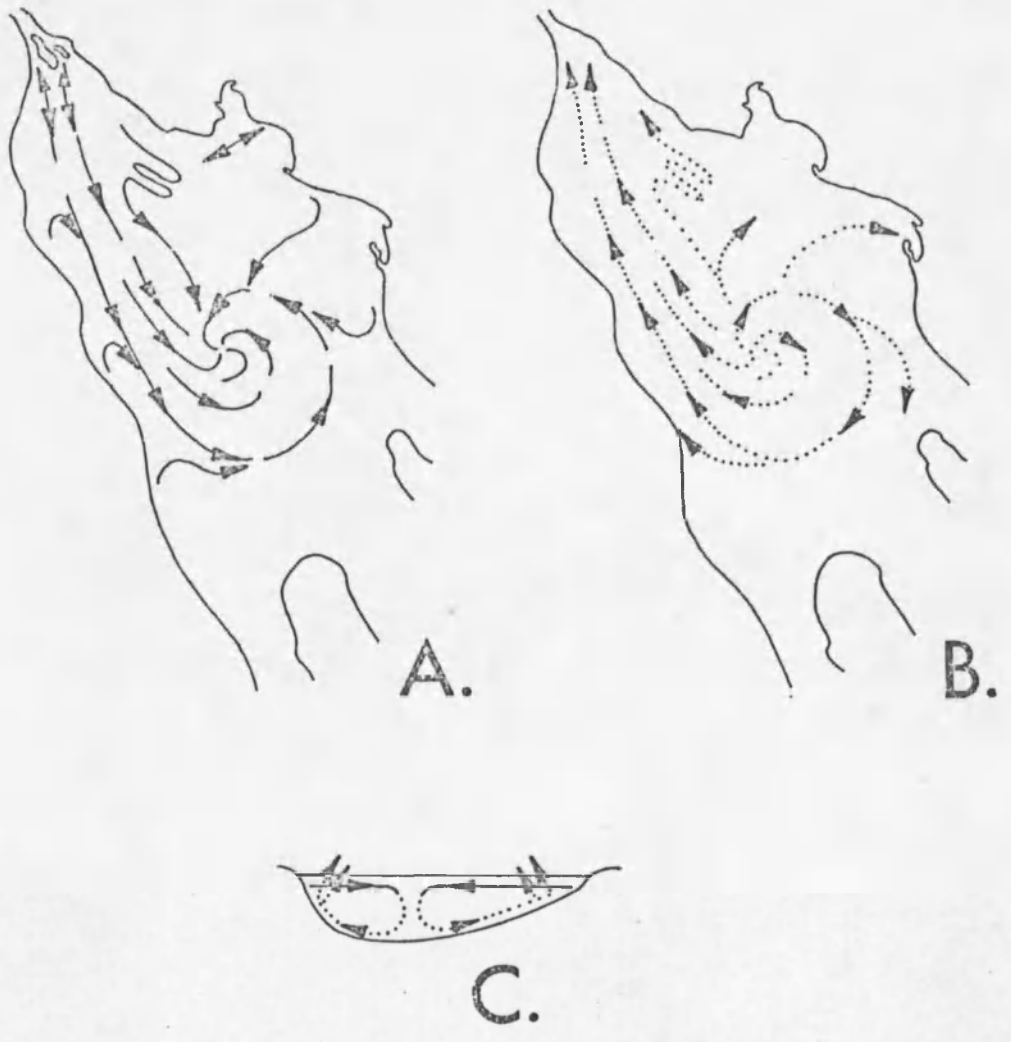

Figure 22. Thermal dynamic model of the Northern Gulf of California during the summer. -- (A) Surface circulation; (B) bottom circulation; (C) east-west section. After Lepley (1973).

would fit that expectation. Figure 23 is an example of such upwelling plumes.

Tides

The study of tides in the Northern Gulf of California is not an easy subject. The reason for this is the lack of primary tidal stations (Puerto Penasco is the only one in the area). Some questions about tidal phase and tidal current velocities in this part of the Gulf of California have not been answered completely. Reports about the natural period of oscillation of the Gulf disagree (Matthews 1969). Tidal current velocities in the area have been measured (Thompson 1969b), but a complete seasonal scheme of these tidal currents is still unavailable.

The analysis of ERTS-1 imagery has provided new information for the study of both tidal phase and tidal current velocities. Figure 24 is a photograph of a composite sandwich overlay consisting of a positive 70 mm transparency of band 7, taken May 21, 1973, over a negative 70 mm transparency of band 7, taken June 8, 1973. This shows only the intertidal zone. Tidal calendars (DGOSM 1973, Thomson 1973) available for Puerto Penasco show that on May 21 the tide was at 0 feet (low tide), and on June 8 the tide was at 10 feet (high tide). The use of ERTS-1 synoptic imagery in this way should allow measurements of tidal phase velocities in this region where access with the instrumentation needed for direct measurement is difficult. Unfortunately, with the imagery available for this thesis, it was not possible to record both extremes of the 20-plus foot vertical excursions of spring tides in the Northern

Figure 23. Plumes of clear water (arrows) near shore. -- Satellite overpass corresponding to September 30, 1972 (band 5).

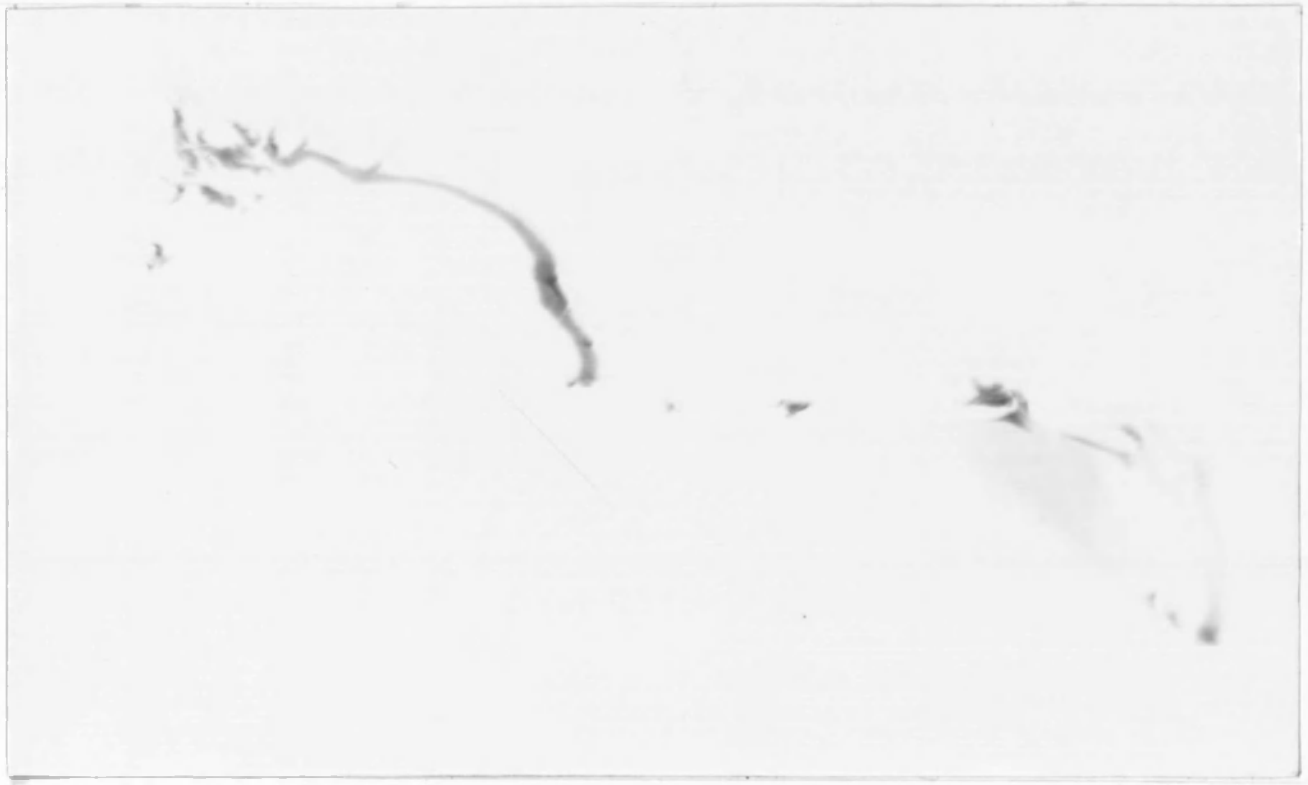

Figure 24. Photographic overlay (positive over negative) to show the intertidal zone. -- Images from May 21 and June 8, 1973.

Gulf because none of the satellite overpasses coincided with the peaks of the spring tides.

The analysis of turbidity banding patterns shown mainly by band 5 in most of the ERTS-1 imagery available for the study was very useful for the indirect measurement of tidal current velocity. Figure 25 shows an example of this phenomenon. The width of this banding pattern, which represents a historical record of the tidal pulses, varies from approximately 5 nautical miles in the northeast along the Sonoran Coast to 20 miles in the southwest along the Baja California coast, giving average net velocities of 0.4 and 1.7 knots, respectively. The differential in velocity on the two sides of the Gulf illustrates a counterclockwise rotary component of net velocity. This agrees with the expected diversion of flow to the right toward the east from the Coriolis effect on this outward flow.

Band 7 of ERTS-1 imagery taken during low points of spring tides is very useful to delineate the intertidal zone. Figure 26 (May 21, 1973) is a good example of this. The exposed intertidal zone is recognizable by its distinct dark gray tone.

Internal Waves

The presence of internal waves in the oceans has long been recognized (Phillips 1966). The unwanted variability frequently found in profile measurements of temperature and salinity has often been attributed to them, particularly near the highly stratified thermocline. This kind of wave, always a subsurface feature, forms at the interface of two strata of water of different density, the surface itself remaining

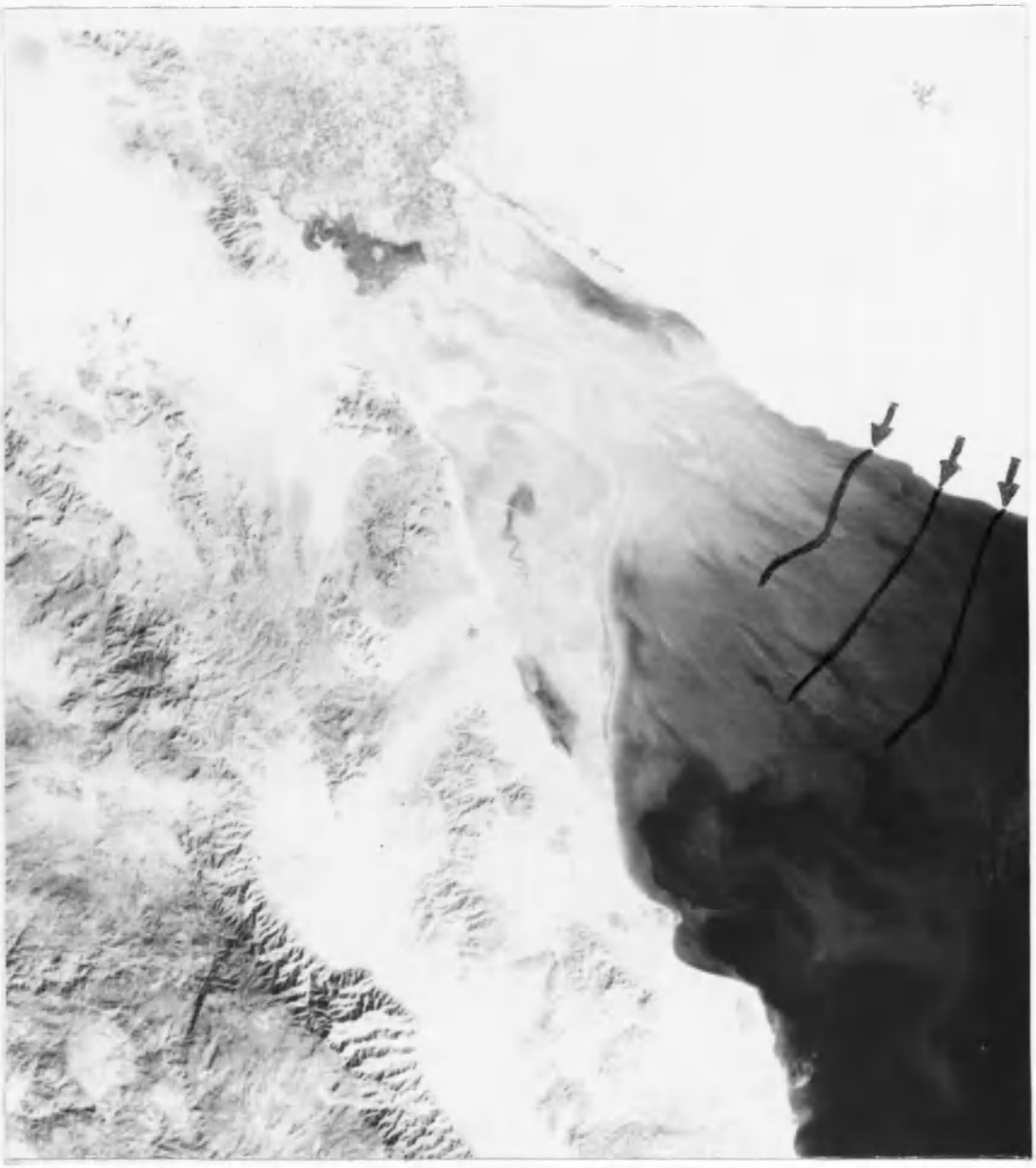

Figure 25. Turbidity banding demonstrating tidal pulses, Northern Gulf of California. -- ERTS-1 image from November 5, 1972, band 5.

Figure 26. Intertidal zone, Adair Bay. -- ERTS-1 image from May 21, 1972, band 7.

almost smooth. For this very reason these oscillations have escaped investigation until fairly recently. Some authors like Defant (1958) have stated that these ocean features cannot be detected from above, but remote sensing may prove the contrary. MSS imagery corresponding to the summer satellites overpasses, show in all of the four bands "ribbons" like features that are believed to be a manifestation of internal wave structures just below the water surface. These cyclically banded patterns with wavelengths of from 2 to 5 kilometers are not oriented with the swell patterns in the area and have a surface signature of slicks that modify the surface. These slicks are generated by the sun glitter effect (solar elevation greater than 60 degrees) over the divergent zones above the crests of internal waves. The necessary interface for the formation of this type of waves would be provided by the buoyant estuarine layers of warmer water described in the summer circulation model. Figure 27 shows two types of internal wave patterns: adjacent and parallel to the west coast of the Northern Gulf, one set appears to occur within a single long mass of estuarine water which eventually curls into a gyre at its southern end in this image. The other type of internal wave pattern in this scene occurs in the mid-gulf as overlapping arcuate sets concave to the west, which may be remnants of older estuarine gyres of previous tidal pulses that have drifted eastward. The fact that these banded wave patterns end abruptly in mid-gulf is taken as evidence that these are indeed internal wave patterns which are breaking against the edges of the floating lenses in which they are contained. If this is true, an answer to the driving mechanism for these internal waves is

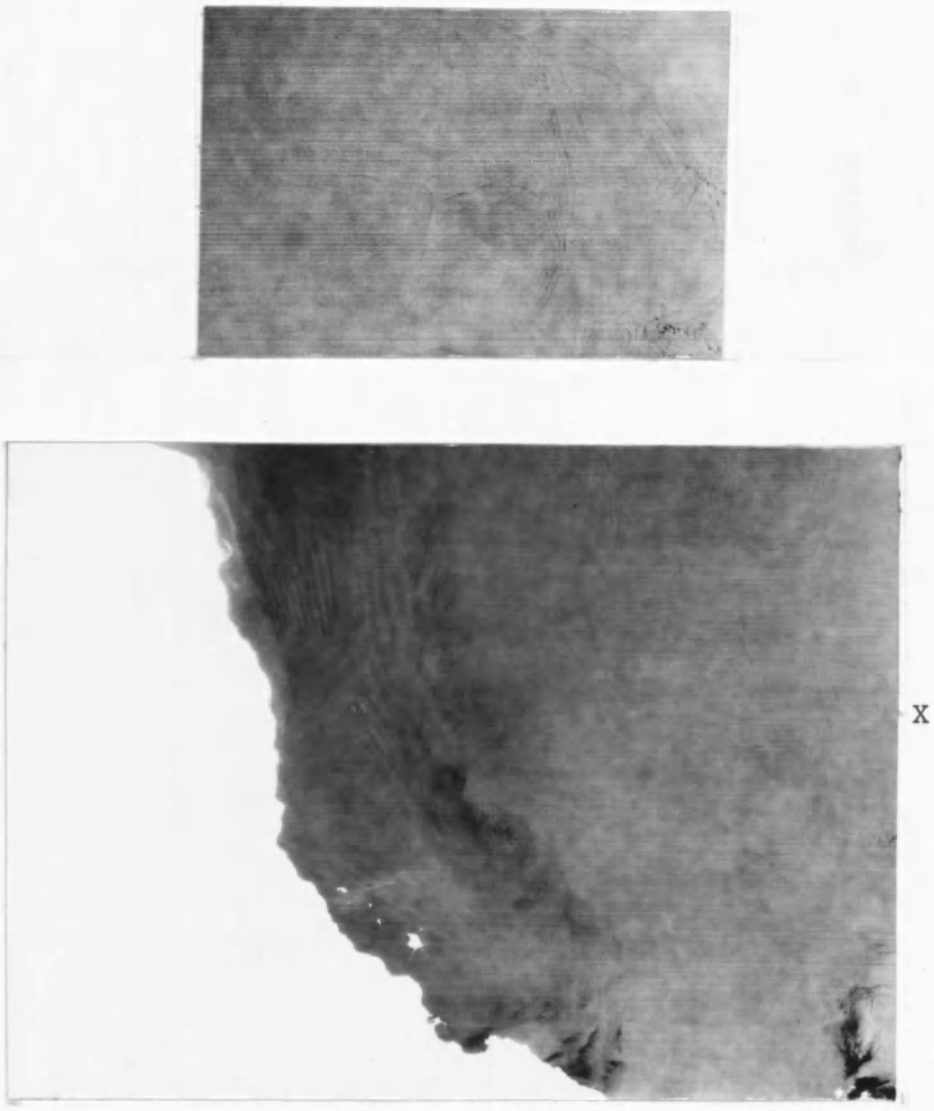

Figure 27. Internal waves, Northern Gulf of California. -- Image of area just north of Angel de la Guarda Island; Baja California coast on left. Upper photo is enlargement of area adjacent to X on lower photo. ERTS-1 image from May 3, 1973, band 5.

also found. The wavelengths of about 5 kilometers that are measured directly on the imagery show that these internal waves are small compared to the internal waves that would be generated by the tidal action (Phillips 1966). This leaves only two possible driving mechanisms: the wind and the flow of the thin layer of warm water (weak vertical shear). The wind, blowing during the summer from the southeast, would explain the arcuate set of internal waves (transfer of momentum to the right of the wind direction) concave to the west, but not the set that appears to occur within the single long mass of estuarine water. The weak vertical shear due to the north-south flow of the warm surface water has the effect of reducing the frequency and vertical scale of small internal wave motions (Phillips 1966). This explains the short wavelengths of the detected internal waves (as compared to longer wavelength expected in tide generated internal waves). The change in the direction of the vertical shear due to the counterclockwise gyre of the warm surface water accounts for the two sets of internal waves under consideration. The vertical motions of these kinds of weak vertical shear generated internal waves are suppressed rapidly (energy is ultimately lost from the waves, being transferred to the mean flow). The motion then becomes almost entirely horizontal. This horizontal motion also dies away but more slowly than the vertical motion. As the vertical scale decreases, however, the vertical gradients of the velocity field continue to increase, leading possibly to a local instability and an accelerated decay of the wave motion by the generation of turbulence (Phillips 1966). Figure 28 shows an hourglass-shaped white blotch about

Figure 28. Hourglass-shaped figure (A), thought to be turbulent water resulting from the breaking of internal waves. -- ERTS-1 imagery corresponding to May 3, 1973, band 7.

9 km in length thought to be turbulent white water. This is in agreement with the vertical shear generated internal waves theory.

Suspended Sediments

Suspended sediment concentrations ranging from 1 ppm to 45 ppm have been measured in the Northern Gulf of California (Alvarez-Borrego et al. 1974, Gayman 1969). Generally, the measured concentrations are higher in the northwest and decrease toward the southeast. On the Sonoran side the waters are less turbid than in the rest of the area. This is thought to be due to the deeper waters (channel running parallel to the coast) and the strong tidal currents in the area.

During the ERTS-1 overpasses Secchi depth readings ranged from about 0.2 meters in the Isla Montague area to about 3 meters in the deep channel (Hendrickson 1973, Alvarez-Borrego et al. 1974). Therefore, it is quite unlikely that the bottom will be visible in any of the ERTS-1 channels and it is possible to say that in the Northern Gulf of California most of the visible features will be caused by light reflected off the surface or backscattered from suspended matter (Austin 1972).

In past experiments in other areas which used aerial and orbital photography to enhance suspended sediment patterns (Klemas, Srna and Treasure 1973; Bowker et al. 1973; Mairs 1970) it has been shown that red filters have been particularly effective for discriminating brown sediment-laden water in shallow areas from the less turbid dark-green waters in deeper areas.

Figure 29 contains MSS images of the Northern Gulf of California (orbits 1032 and 1033) in the four bands. Suspended sediment patterns

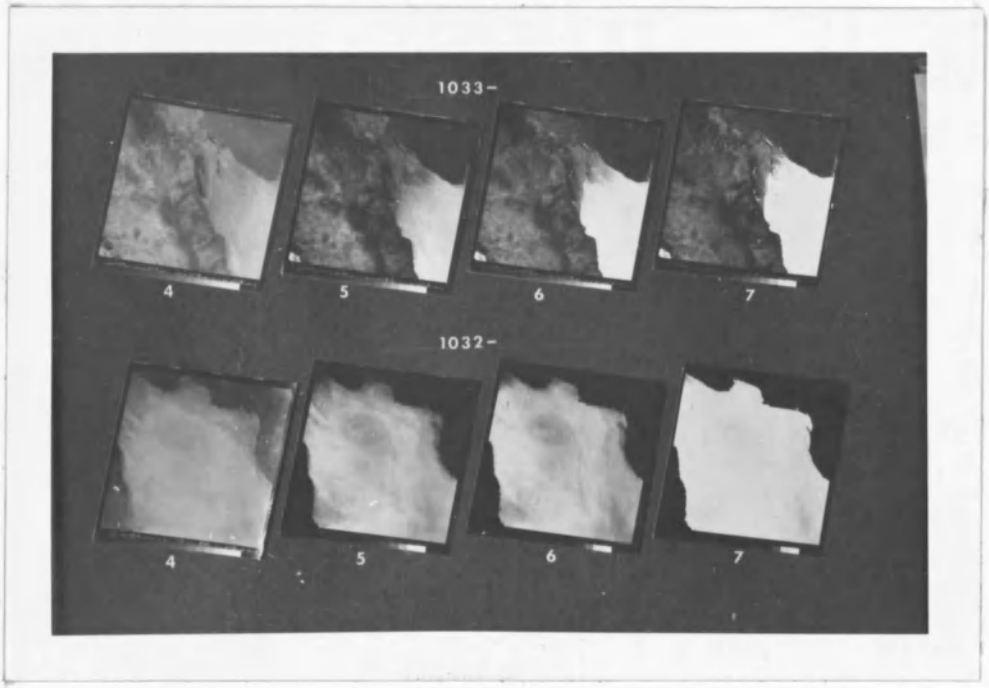

Figure 29. Suspended sediments are shown better in band 5 of these multispectral quadrants (August 24 and 25, 1972).

appear most distinct in band 5, the red channel which agrees with aircraft and orbital results. Band 4 displays a more complex pattern of suspended matter, which is further aggravated by a masking effect resembling scattering by the atmosphere or haze. Due to its limited water penetration, band 6 and band 7 show only weak patterns of suspended sediment near the surface.

Wind Effects Upon Surface Layers

Wind-induced drift of the warmer surface layers are evident when meteorological data is compared with the imagery. For example, in Figure 30A and 30B of August 24 and 25, 1972, a 12.2 knot southwest wind (Hendrickson 1973) has pushed the cyclonic surface gyre and other turbid surface layers northeasterly whereas the multispectral quadrant of Figure 31 (September 12, 1972) show the estuarine layer plastered against the western shore by a 3.5 knot northeasterly wind.

Orographic Indicator of a Shoal

Figure 32 (August 7, 1972) shows a disturbance of incoming laminar tidal flow water. It appears that the estuarine layer has been torn by a subsurface protrusion. The point of the plume coincides with the mapped location of a shoal on the U. S. Naval Oceanographic Office Chart 620 (see also Figure 4).

Runoff

On the imagery for March 10, 1973, a floating sheet of rainwater was made visible by the slight increase in surface turbidity, onshore evidence of rain in the area, and a cloud-line indicating a temperature

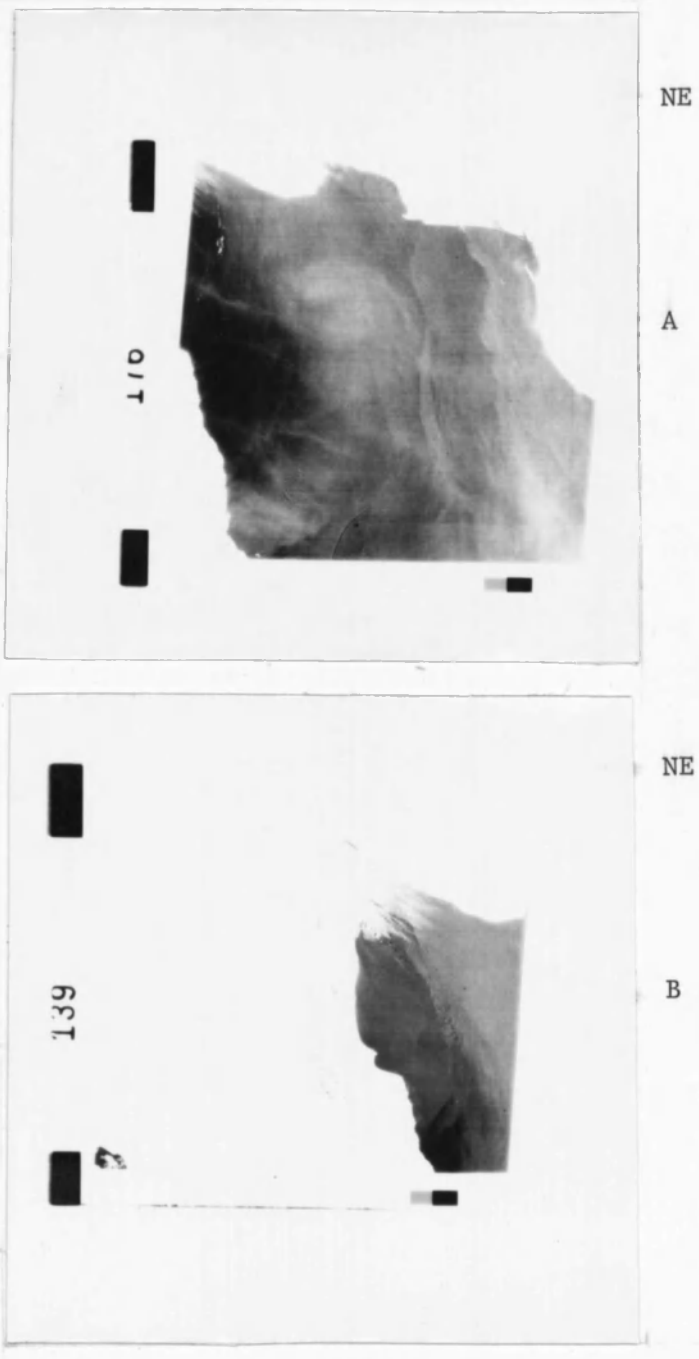

Figure 30. Wind effects on surface layers, Northern Gulf of California. -- August 24 (A) and August 25 (B), 1972.

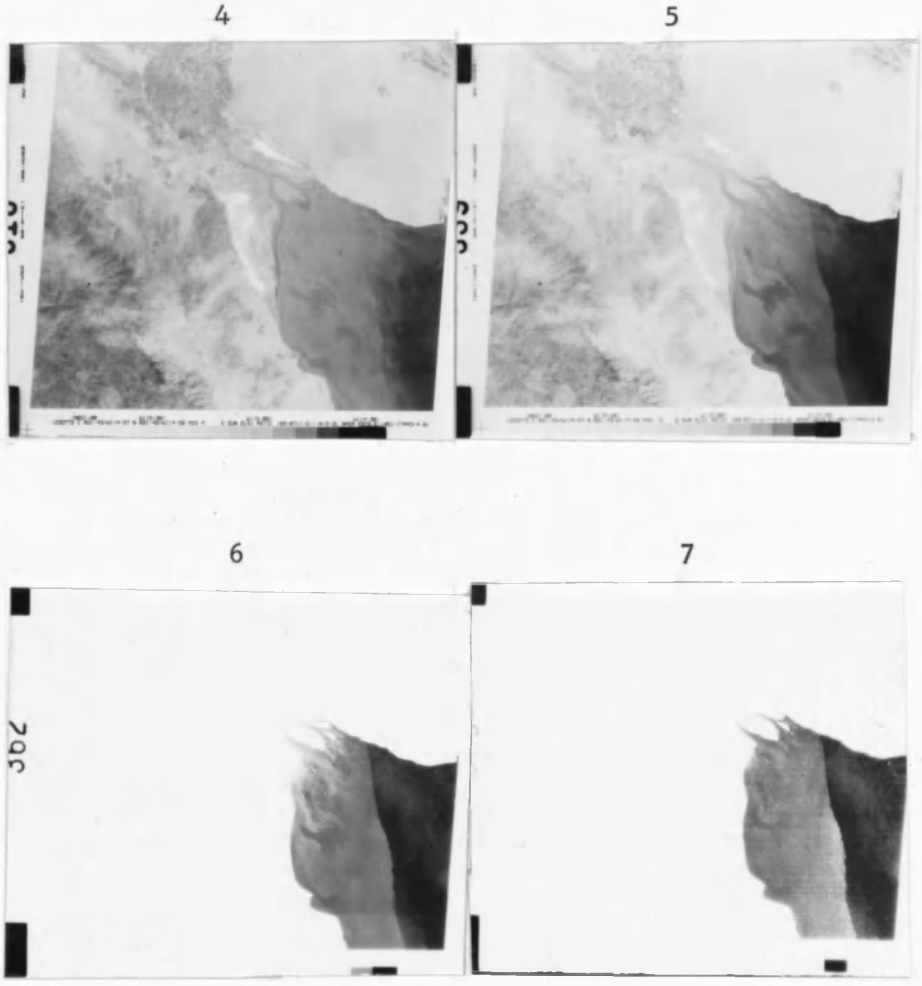

Figure 31. Strong northeasterly wind pushing surface layers against west shore of the Northern Gulf of California. -- ERTS-1 images from September 12, 1972.

Figure 32. Orographic indicator of a shoal (arrow). -- Image from August 7, 1972, band 6.

step at the boundary of the turbid layer. Figure 33 A, 33B and 33C shows pairs of images from February 20, March 10, and March 28, 1973, in which band 7 images were enhanced for land and water respectively. The sequential images show (1) cloudy weather previous to March 10, (2) the presence of the runoff layer at sea on March 10, and (3) the absence of this layer by March 28. It also compares the high albedo of the adjacent desert areas shown in the March 28 image with the dark tones of the moist soil in the March 10 image.

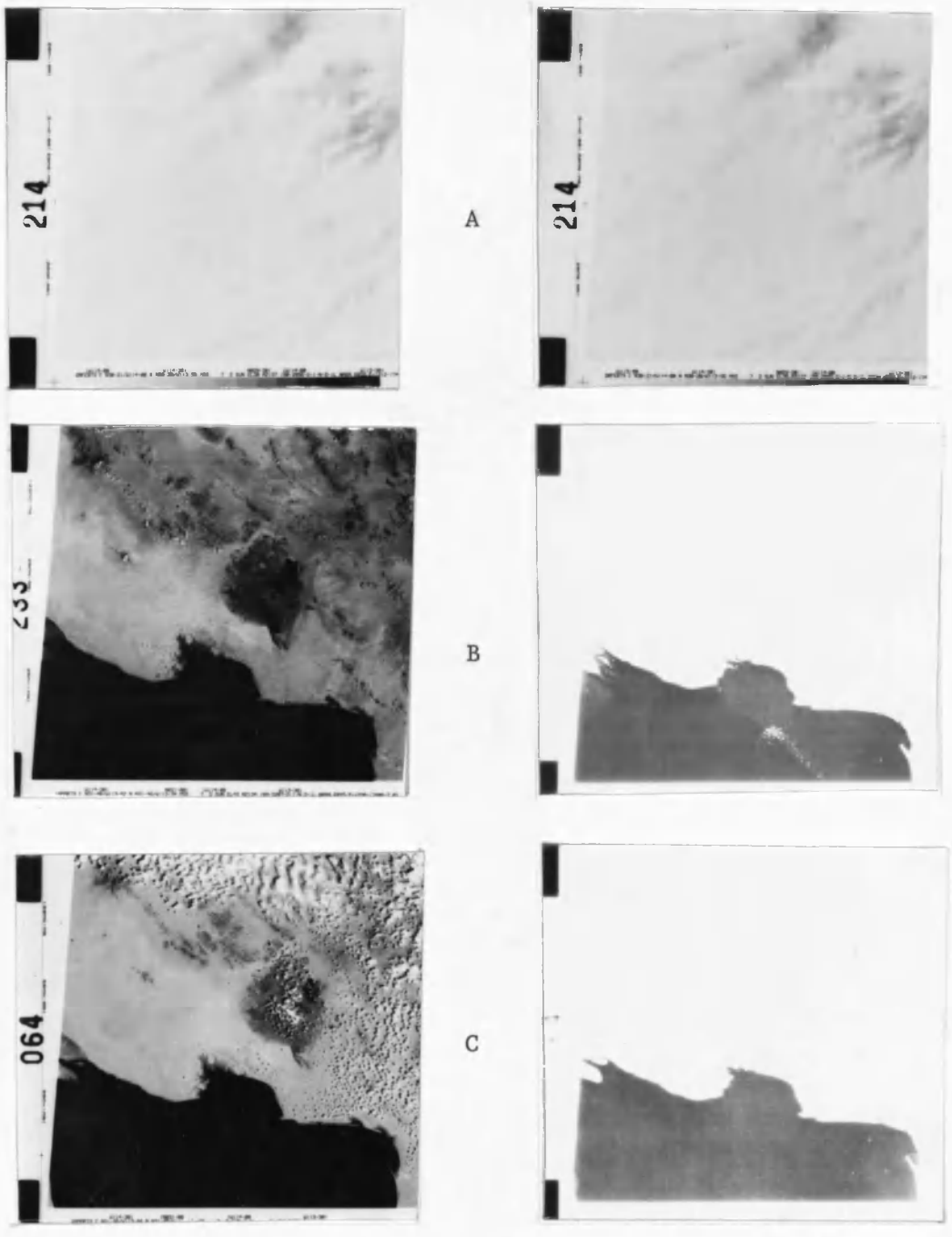

Figure 33. History of rainfall and runoff, Northern Gulf of California. -- Figures on left enhanced for land, figures on right enhanced for water. (A) February 20, 1973, cloudy weather; (B) March 10, 1973, runoff layer at sea; (C) March 28, 1973, runoff layer gone.

CONCLUSIONS

1. Detection of the dynamic oceanographic parameters of the Northern Gulf of California and its seasonal changes using ERTS-1 data is possible due mainly to the cloud-free atmosphere that prevails over the area most of the time. Twenty-nine out of 40 ERTS-1 satellite overpasses in one year over the northern Gulf were successful.
2. The lack of direct information from great depths using ERTS-1 imagery is offset by the amount of high resolution synoptic data from the top meters given by the same imagery, impossible to obtain otherwise.
3. Surface circulation patterns in the Northern Gulf of California during the summer (May through October) are easily detected on ERTS-1 imagery due to the load of suspended sediment that acts as a natural tracer. During the winter (November through April) the surface waters appear clear (band 6 and band 7) making difficult the study of the circulation patterns in the area.
4. A seasonal circulation model developed during the interpretation of one year of ERTS-1 data for the area of study, agrees with several of the oceanographic parameters detected in the area: counterclockwise gyres, upwelling plumes, and internal waves.
5. The changes in the distribution and configuration of tidal flats in the Northern Gulf of California can be monitored with MSS

band 7 images. The measuring of the tidal flat itself provides information about the tidal phase velocity in the area in which there are not primary tidal stations in operation. The knowledge of the tidal flats configuration is essential for the management of clam beds known to exist there.

6. From the analyses of the imagery and taking into account that the discharge of the Colorado River is negligible, it is concluded that tidal activity is the responsible for the high turbidity levels in the estuarine area. Tidal pulsations detected by means of turbidity banded patterns, shown best by MSS band 5 allow and indirect estimate of tidal current velocities.
7. ERTS-1 MSS band 5 (0.6-0.7 microns) gives the sharpest definition of interface between waters of different turbidity. Band 4 (0.5-0.6 micron), due to its deeper water penetration, is more sensitive to patterns having lower turbidity, yet was veiled by a uniform blanket of atmospheric scattering making identification of sediment patterns more difficult. Band 6 (0.7-0.8 microns) and band 7 (0.8-1.1 microns) clearly delineate the shoreline and discriminates water from land.
8. Sun glint patterns, produced when the sun elevation angle is greater than 60 degrees above the horizon, permitted the detection of internal waves although other water surface features are obscured by the same effect.
9. The use of spectroradiometric data in the analysis of ERTS-1 data together with surface truth data like secchi disk, turbidity

and plankton content, make possible the classification of different types of water according to its spectral reflectance properties.

RECOMMENDATIONS

The present study has shown that the detection of oceanographic features of the Northern Gulf of California and its seasonal variations using ERTS data are possible. The results obtained during this project are considered to be representative of a typical year in the area. Therefore, the continuation of the study in a long term basis is advisable. For this long term study, imagery from ERTS-1 and ERTS-2 would be available.

The correlation of spectral properties to various surface-identified water types indicate that computer mapping from the ERTS-1 and ERTS-2 (to be launched in 1976) MSS digital tapes will be possible. It is therefore recommended that for future studies of the area using ERTS data, the computer mapping method be included within the analysis techniques.

Due to the large magnitude of the tidal excursions in the Northern Gulf of California, surface truth transects should be acquired over a distance of 150 km within a total time of about two hours. These should include spectral radiometric readings for calibrating multispectral imagery, which are obtained from sufficient height above the water surface to obtain an integration of the specular flashes from surface waves. The most practical and economical means of meeting these two requirements is the use of aircraft. A seaplane or float plane can carry

continuously recording optical and thermal radiometers. Mexican or United States commercial aircraft could be chartered for this purpose.

Practical and immediate use of ERTS-1 imagery include:

1. Estimations of the total producing area of the clam beds known to exist in the intertidal zone (mud flats). These estimations should be of utility in managing the resource.
2. Monitoring sites for suspected pesticide and heavy metal contamination.
3. Corrections of the nautical charts of the area adding on these the low tide and the high tide shorelines.

APPENDIX A

SPECTRORADIOMETRIC AND SECCHI DISK DATA

The downwelling and upwelling radiance readings are in an arbitrary radiance scale.

Date Station	Band	Downwelling Radiance Dw	Upwelling Radiance Uw	Relative Reflectance (Uw/Dw)	Secchi Disk Reading (meters)
01/14/73 A-1	4	28	1.12	0.040	8.0
	5	39	0.76	0.020	8.0
	6	30	0.64	0.020	8.0
	7	42	1.12	0.030	8.0
01/14/73 A-2	4	28	2.30	0.080	5.2
	5	36	0.96	0.030	5.2
	6	29	0.24	0.008	5.2
	7	34	0.32	0.009	5.2
01/14/73 B-12	4	18	3.70	0.200	5.0
	5	22	2.50	0.114	5.0
	6	28	0.56	0.020	5.0
	7	37	0.50	0.013	5.0
01/15/73 A-9	4	82	0.84	0.010	17.0
	5	24	0.66	0.027	17.0
	6	20	0.50	0.025	17.0
	7	24	0.66	0.027	17.0
01/15/73 B-3	4	32	0.90	0.028	25.0
	5	42	0.90	0.021	25.0
	6	32	0.53	0.016	25.0
	7	52	0.80	0.015	25.0
01/15/73 B-2	4	15	1.25	0.084	15.0
	5	28	0.72	0.026	15.0
	6	17	0.64	0.037	15.0
	7	38	0.50	0.013	15.0

Date Station	Band	Downwelling Radiance Dw	Upwelling Radiance Uw	Relative Reflectance (Uw/Dw)	Secchi Disk Reading (meters)
01/16/73 E-1	4	11	0.87	0.079	14.0
	5	13	0.76	0.058	14.0
	6	10	0.48	0.048	14.0
	7	14	0.72	0.051	14.0
01/16/73 B-5	4	21	1.08	0.051	14.0
	5	22	1.00	0.045	14.0
	6	18	0.80	0.044	14.0
	7	26	0.96	0.037	14.0
01/16/73 B-8	4	28	1.48	0.051	9.0
	5	36	0.76	0.019	9.0
	6	28	0.68	0.024	9.0
	7	39	0.72	0.018	9.0
01/17/73 B-9	4	31	2.00	0.064	5.0
	5	40	0.92	0.023	5.0
	6	28	0.36	0.012	5.0
	7	46	0.68	0.014	5.0
01/18/73 C-6	4	22	7.60	0.344	2.0
	5	30	4.20	0.139	2.0
	6	24	0.56	0.023	2.0
	7	40	0.40	0.010	2.0
01/18/73 C-8	4	13	6.20	0.475	1.0
	5	14	5.60	0.400	1.0
	6	15	6.00	0.400	1.0
	7	28	0.68	0.024	1.0

Date Station	Band	Downwelling Radiance Dw	Upwelling Radiance Uw	Relative Reflectance (Uw/Dw)	Secchi Disk Reading (meters)
01/19/73 D-4	4	22	10.60	0.480	0.1
	5	30	18.0	0.600	0.1
	6	26	17.00	0.650	0.1
	7	38	22.00	0.600	0.1
01/19/73 D-3	4	14	9.20	0.650	0.2
	5	19	13.00	0.680	0.2
	6	16	8.60	0.530	0.2
	7	24	8.00	0.334	0.2
01/21/73 E-2	4	19	1.10	0.058	7.0
	5	26	0.56	0.021	7.0
	6	18	0.24	0.013	7.0
	7	37	0.20	0.005	7.0
03/27/73 D-8	4	46	4.00	0.091	4.2
	5	58	2.00	0.034	4.2
	6	44	1.00	0.022	4.2
	7	66	1.01	0.017	4.2
04/15/73 C-6	4	22	4.00	0.182	2.8
	5	29	3.60	0.124	2.8
	6	22	0.66	0.033	2.8
	7	30	0.32	0.010	2.8
04/15/73 D-8	4	38	5.10	0.146	1.3
	5	48	4.00	0.083	1.3
	6	36	0.80	0.022	1.3
	7	54	0.66	0.011	1.3

Date	Station	Band	Downwelling Radiance Dw	Upwelling Radiance Uw	Relative Reflectance (Uw/Dw)	Secchi Disk Reading (meters)
04/16/73	C-7	4	46	8.20	0.200	0.4
		5	60	10.20	0.193	0.4
		6	46	4.00	0.087	0.4
		7	66	2.40	0.036	0.4
04/16/73	D-9	4	54	12.10	0.250	0.3
		5	64	18.00	0.280	0.3
		6	48	6.04	0.132	0.3
		7	82	7.20	0.088	0.3
04/15/73	D-7	4	50	10.40	0.207	0.5
		5	65	12.00	0.190	0.5
		6	52	3.12	0.062	0.5
		7	78	1.67	0.021	0.5
06/7/73	A-1	4	50	8.12	0.184	5.0
		5	62	6.20	0.116	5.0
		6	50	4.00	0.080	5.0
		7	82	4.40	0.054	5.0
06/7/73	A-2	4	42	2.70	0.065	5.0
		5	54	1.28	0.024	5.0
		6	48	0.40	0.008	5.0
		7	54	0.40	0.007	5.0
06/7/73	A-6	4	30	2.22	0.075	5.0
		5	40	1.04	0.026	5.0
		6	36	0.32	0.009	5.0
		7	42	0.23	0.005	5.0

Date	Station	Band	Downwelling Radiance Dw	Upwelling Radiance Uw	Relative Reflectance (Uw/Dw)	Secchi Disk Reading (meters)
06/7/73	A-1	4	52	6.00	0.118	9.5
		5	65	8.40	0.128	9.5
		6	54	4.00	0.074	9.5
		7	84	5.60	0.066	9.5
06/7/73	A-10	4	54	2.63	0.049	12.4
		5	65	1.68	0.026	12.4
		6	54	1.04	0.019	12.4
		7	84	1.12	0.132	12.4
06/9/73	A-8	4	32	1.52	0.047	15.0
		5	40	0.80	0.020	15.0
		6	30	0.48	0.016	15.0
		7	38	0.40	0.010	15.0
06/9/73	A-9	4	44	1.20	0.027	15.0
		5	64	0.96	0.015	15.0
		6	44	0.56	0.012	15.0
		7	66	0.56	0.008	15.0
06/9/73	B-2	4	56	6.80	0.121	16.0
		5	74	5.20	0.071	16.0
		6	58	4.00	0.069	16.0
		7	80	3.20	0.040	16.0
06/9/73	B-3	4	58	4.40	0.076	15.0
		5	73	5.20	0.072	15.0
		6	22	4.40	0.073	15.0
		7	40	8.00	0.085	15.0

Date	Station	Band	Downwelling Radiance Dw	Upwelling Radiance Uw	Relative Reflectance (Uw/Dw)	Secchi Disk Reading (meters)
06/9/73	B-6	4	48	1.12	0.023	15.0
		5	62	0.56	0.009	15.0
		6	50	0.40	0.008	15.0
		7	74	0.48	0.006	15.0
06/9/73	B-10	4	24	0.80	0.033	16.0
		5	34	0.40	0.011	16.0
		6	30	0.40	0.013	16.0
		7	42	0.41	0.010	16.0
06/10/73	B-9	4	50	4.00	0.016	10.0
		5	66	0.88	0.013	10.0
		6	52	0.40	0.007	10.0
		7	80	0.48	0.006	10.0
06/10/73	D-4	4	36	14.00	0.390	0.3
		5	50	20.00	0.400	0.3
		6	40	10.40	0.260	0.3
		7	57	1.00	0.123	0.3
06/10/73	B-12	4	32	2.50	0.079	6.0
		5	40	1.02	0.042	6.0
		6	34	0.40	0.012	6.0
		7	45	0.40	0.001	6.0
06/11/73	D-2	4	28	7.60	0.270	0.3
		5	34	9.20	0.272	0.3
		6	27	4.00	0.148	0.3
		7	38	3.60	0.095	0.3

Date Station	Band	Downwelling Radiance Dw	Upwelling Radiance Uw	Relative Reflectance (Uw/Dw)	Secchi Disk Reading (meters)
06/11/73 D-3	4	54	8.00	0.148	0.5
	5	68	10.00	0.148	0.5
	6	54	4.60	0.085	0.5
	7	80	4.00	0.050	0.5
06/11/73 D-5	4	16	10.00	0.622	0.5
	5	20	14.00	0.700	0.5
	6	16	6.00	0.373	0.5
	7	24	5.02	0.216	0.5
06/11/73 D-5	4	25	8.00	0.320	0.5
	5	29	8.14	0.336	0.5
	6	20	4.00	0.200	0.5
	7	28	3.02	0.115	0.5

REFERENCES

Alvarez-Borrego, S., K. Nishikawa-Kinomura and G. Florez-Muñoz. 1974. Final report to the secretariat of hydraulic resources on the chemical study on insecticide contamination at the mouth of the Colorado River. Marine Sciences Unit, Inst. of Oceanologic Research, Ensenada, Baja California, Mexico.

Austin, R. W. 1972. Surface truth measurements of optical properties of the waters in the Northern Gulf of California. In Fourth Annual Earth Resources Program Review, Vol. 4, Sect. 106:1-9, NASA Manned Spacecraft Center, Houston, Texas.

Badgley, P. C., L. Miloy and L. Childs. 1968. Oceans from Space, Gulf Publishing Company, Houston, Texas.

Beal, C. H. 1948. Reconnaissance of the geology and oil possibilities of Baja California, Mexico. Geol. Soc. America Mem. 31, 138 pp.

Bowker, D. E., P. Fleischer, T. A. Gosiak, W. J. Hanna and J. Ludwich. 1973. Correlation of ERTS-1 multispectral imagery with suspended matter and chlorophyll in lower Chesapeake Bay. Symp. Significant Results Obtained from ERTS-1, NASA Goddard S.F.C., Greenbelt, Maryland, March 5-9.

Comite de la Carta Geologica de Mexico. 1960. Carta geologica de la Republica Mexicana (scale 1:2,000,000).

Defant, A. 1958. Ebb and Flow. The University of Michigan, Ann Arbor.

DGOSM. 1973. Calendario de Mareas para Puerto Penasco, Son. Direccion General de Oceanografia y Senalamiento Maritimo, Secretaria de Marina, Mexico.

Duntley, S. Q. 1972. Detection of ocean chlorophyll from earth orbit. In Fourth Annual Earth Resources Program Review, Vol. 4, Sect. 102:1, NASA Manned Spacecraft Center, Houston, Texas.

Emilsson, I. 1972. Elementos de Oceanografia Fisica, Apuntes no Publicados, Instituto de Geofisica de la Universidad Nacional Autonoma de Mexico, Mexico D.F.

Filloux, J. H. 1972. Tides in the Gulf of California, Scripps Institution of Oceanography, University of California, San Diego La Jolla California.

Gayman, W. 1969. Turbidity in the extreme Northern Gulf of California. In D. A. Thomson, A. R. Mead and J. R. Schreiber, Jr. (eds.) Environmental impact of brine effluents on Gulf of California. U. S. Department of Interior, Office of Saline Water, Research and Development Progress Report No. 387, pp. 88-91.

Green, C. R. 1969. Meteorological conditions. In D. A. Thomson, A. R. Mead and J. R. Schreiber, Jr. (eds.) Environmental impact of brine effluents on Gulf of California. U. S. Department of Interior, Office of Saline Water, Research and Development Progress Report No. 387, pp. 7-15.

Hendrickson, J. R. 1973. Study of the marine environment of the Northern Gulf of California, Goddard Space Flight Center, Type III Final Report.

Klemas, V., R. Srna and W. Treasure. 1973. Applicability of ERTS-1 imagery to the study of suspended sediment and aquatic fronts. Symp. Significant Results obtained from ERTS-1, NASA-Goddard S.F.C., Greenbelt, Maryland.

Lepley, L. K. 1968. Coastal water clarity from space photographs. Photogrammetric Engineering, 34(7):667-674.

Lepley, L. K. 1973. ERTS imagery analysis. In J. R. Hendrickson (ed.) Study of the marine environment of the Northern Gulf of California, Goddard Space Flight Center, Type III Final Report, pp. 70-95.

Lepley, L. K., J. R. Hendrickson and G. Calderon. 1973. Oceanographic mapping of structure and dynamics of the Northern Gulf of California by the use of spectral modeling and ERTS-1. Symp. on significant results obtained from the Earth Resources Technology Satellite-1, Vol. I, Sect. B:1349-1357.

Mairs, R. L. 1970. Oceanographic interpretation of Apollo photographs. Photogrammetric Engineering, Vol. XXXVI, No. 10, Oct. 1970, pp. 1045-1058.

Matthews, J. B. 1969. Tides in the Gulf of California. In D. A. Thompson, A. R. Mead and J. R. Schreiber, Jr. (eds.) Environmental impact of brine effluents on Gulf of California. U. S. Department of Interior, Office of Saline Water, Research and Development Progress Report No. 387, pp. 41-50.

Merrit, E. and A. S. Stancioff. 1971. Satellite oceanography. Underwater Journal, December 1971, pp. 250-262.

NASA. 1972. ERTS-1 User's manual. Goddard Space Flight Center, Greenbelt, Maryland.

Phillips, O. M. 1966. The dynamics of the upper ocean. Cambridge, England, The University Press.

Ross, D. S. 1969. Report on Ben Franklin spectral filter tests, Philco-Ford Corporation prepared for U. S. Naval Oceanographic Office.

Schreiber, J. R., Jr. 1969a. Changes in Colorado River flow. In D. A. Thompson, A. R. Mead and J. R. Schreiber, Jr. (eds.) Environmental impact of brine effluents on Gulf of California. U. S. Department of Interior, Office of Saline Water, Research and Development Progress Report No. 387, pp. 83-87.

Schreiber, J. R., Jr. 1969b. Geographical and geological features. In D. A. Thompson, A. R. Mead and J. R. Schreiber, Jr. (eds.) Environmental impact of brine effluents on Gulf of California. U. S. Department of Interior, Office of Saline Water, Research and Development Progress Report No. 387, pp. 3-6.

Sverdrup, H. U., M. W. Johnson and R. H. Fleming. 1963. The Oceans: Their Physics, Chemistry and General Biology. Prentice-Hall, Inc., pp. 84-85.

Sykes, G. 1937. The Colorado delta. Carnegie Institute, Washington. Pub. No. 460, 193 pp.

Thackrey, D. E. 1968. Research in infrared sensing. Research News, 18:1-12, February 1968.

Thompson, R. W. 1965. Tidal flat sedimentation on the Colorado River delta, Northerwestern Gulf of California. San Diego, California, University of California, Scripps Institution of Oceanography (Unpublished Ph. D. dissertation), 245 pp.

Thompson, R. W. 1969a. Bathymetry and sedimentation. In D. A. Thompson, A. R. Mead and J. R. Schreiber, Jr. (eds.) Environmental impact of brine effluents on Gulf of California. U. S. Department of Interior, Office of Saline Water, Research and Development Progress Report No. 387, pp. 72-82.

Thompson, R. W. 1969b. Tidal currents and general circulation. In D. A. Thompson, A. R. Mead and J. R. Schreiber, Jr. (eds.) Environmental impact of brine effluents on Gulf of California. U. S. Department of Interior, Office of Saline Water, Research and Development Progress Report No. 387, pp. 51-55.

Thomson, D. A. 1972. Tide Calendar for the northern Gulf of California. The University of Arizona, Tucson.

Thomson, D. A. 1973. Tide Calendar for the northern Gulf of California. The University of Arizona, Tucson.

Tyler, J. E. and R. C. Smith. 1970. Measurements of Spectral Radiance Underwater, Gordon and Breach, New York.

White, P. G. 1972. A technique for the reduction and analysis of ocean spectral data. In Fourth Annual Earth Resources Program Review, Vol. 4, Sect. 103.

Williams, J. 1970. Optical Properties of the Sea. U. S. Naval Institute Series in Oceanography, Annapolis, Maryland.